

1

2       **The entorhinal cortex modulates trace fear memory**  
3       **formation and neuroplasticity in the lateral amygdala**  
4                       **via cholecystokinin**

5

6 Hemin Feng<sup>1,2</sup>, Junfeng Su<sup>1,2†</sup>, Wei Fang<sup>1</sup>, Xi Chen<sup>1,2</sup>, and Jufang He<sup>1,2\*</sup>

7 <sup>1</sup>Departments of Biomedical Sciences, and Neuroscience, City University of Hong Kong, Hong  
8 Kong, China

9 <sup>2</sup>City University of Hong Kong Shenzhen Research Institute, Shenzhen, Guangzhou, China

10 \*Corresponding author (jufanghe@cityu.edu.hk)

11 †Current address: F.M. Kirby Neurobiology Center, Boston Children's Hospital, Harvard 22  
12 Medical School, Boston, MA 02115, USA

## 13 Abstract

14 Although the neural circuitry underlying fear memory formation is important in fear-related  
15 mental disorders, it is incompletely understood. Here, we utilized trace fear conditioning to  
16 study the formation of trace fear memory. We identified the entorhinal cortex (EC) as a critical  
17 component of sensory signaling to the amygdala. Moreover, we used the loss of function and  
18 rescue experiments to demonstrate that release of the neuropeptide cholecystinin (CCK)  
19 from the EC is required for trace fear memory formation. We discovered that CCK-positive  
20 neurons extend from the EC to the lateral nuclei of the amygdala (LA), and inhibition of CCK-  
21 dependent signaling in the EC prevented long-term potentiation of sensory signals to the LA  
22 and formation of trace fear memory. Altogether, we suggest a model where sensory stimuli  
23 trigger the release of CCK from EC neurons, which potentiates sensory signals to the LA,  
24 ultimately influencing neural plasticity and trace fear memory formation.

## 25 Introduction

26 Learning to associate environmental cues with subsequent adverse events is an important  
27 survival skill. Pavlovian fear conditioning is widely used to study this association and is  
28 performed by pairing a neutral stimulus (conditioned stimulus, CS), such as a tone, with a  
29 punishing stimulus (unconditioned stimulus, US), such as a shock (Pavlov, 1927). The CS-US  
30 pair elicits fear behaviors, including freezing and fleeing, which are often species-specific.  
31 Canonical delay fear conditioning is performed by terminating the CS and US at the same time.  
32 However, conditioned and unconditioned stimuli do not necessarily occur simultaneously in  
33 nature, and the brain has evolved mechanisms to associate temporally distinct events. Trace  
34 fear conditioning is used to study these mechanisms by inserting a trace interval between the  
35 end of the CS and the beginning of the US. The temporal separation between the CS and the  
36 US substantially increases the difficulty of learning as well as the recruitment of brain  
37 structures (Crestani et al., 2002; Runyan et al., 2004). Although trace fear conditioning  
38 provides essential insight into the neurobiology of learning and memory, many unanswered  
39 questions remain. For instance, the detailed neural circuitry underlying the formation of this  
40 trace fear memory and the potential modulatory chemicals involved in this process need to be  
41 further characterized.

42 Synaptic plasticity is the basis of learning and memory and refers to the ability of neural  
43 connections to become stronger or weaker. Long-term potentiation (LTP) is one of the most  
44 widely-studied forms of synaptic plasticity. The lateral nucleus of the amygdala (LA) receives  
45 multi-modal sensory inputs from the cortex and thalamus and relays them into the central  
46 nucleus of the amygdala (CeA), which then innervates the downstream effector structures  
47 (Phelps & LeDoux, 2005). LTP is developed in the auditory input pathway that signals to the  
48 LA. Auditory-responsive units in the LA fire faster after auditory-cued fear conditioning (Quirk  
49 et al., 1995). Optogenetic manipulation of the auditory input terminals in the LA leads to the  
50 suppression or recovery of LTP in the LA and can correspondingly suppress or recover  
51 conditioned fear responses (Nabavi et al., 2014). Together, these studies demonstrate that  
52 synaptic plasticity in the LA is impressively correlated with the formation of fear memory.

53 In addition to the amygdala, other neural regions, including the hippocampus (Bangasser, 2006),  
54 anterior cingulate cortex (ACC) (Han et al., 2003), medial prefrontal cortex (mPFC) (Runyan  
55 et al., 2004), and entorhinal cortex (EC) (Ryou et al., 2001), take part in trace fear conditioning.

56 The EC is integrated in the spatial and navigation systems of the animal (Fyhn et al., 2004;  
57 Hafting et al., 2005) and is essential for context-related fear associative memory (Maren &  
58 Fanselow, 1997). Moreover, the EC functions as a working memory buffer in the brain to hold  
59 information for temporal associations (Fransén, 2005; Schon et al., 2016). Here, a scenario of  
60 the dependence on the EC to associate the temporally-separated CS and US is manifested.

61 The neuropeptide cholecystokinin (CCK) is universally accepted as the most abundant  
62 neuropeptide in the central nervous system (CNS) (Rehfeld, 1978). CCK is recognized by two  
63 receptors in the CNS: CCK A receptor (CCKAR) and CCK B receptor (CCKBR). Previous  
64 studies in our laboratory unveiled that CCK and CCKBR enabled neuroplasticity as well as  
65 associative memory between two sound stimuli and between visual and auditory stimuli in the  
66 auditory cortex (X. Chen et al., 2019; Li et al., 2014; Z. Zhang et al., 2020). CCK and its  
67 receptors are intrinsically involved in fear-related mental disorders including anxiety (Q. Chen  
68 et al., 2006), depression (Shen et al., 2019), and post-traumatic stress disorder (PTSD) (Joseph  
69 et al., 2013). Moreover, the CCKBR agonist CCK-tetrapeptide (CCK-4) induces acute panic  
70 attacks in individuals with a panic disorder as well as in healthy human subjects (Bradwejn,  
71 1993). Despite the clear connection between CCK and fear-related disorders, it remains elusive  
72 that the involvement of CCK in Pavlovian fear conditioning and the formation of cue-specific  
73 fear memory, which is possibly the neural foundation of these disorders.

74 In the present study, we investigated the involvement of CCK-expressing neurons in the EC in  
75 trace fear memory formation. We then examined how CCK enabled neuroplasticity in the  
76 auditory pathway to the LA by conducting the *in vivo* recording in the LA. Finally, we studied  
77 the contribution of the pathway from the EC to LA on the formation of trace fear memory in a  
78 physiological and behavioral context.

## 79 **Results**

### 80 **Loss of CCK results in deficient trace fear memory formation in CCK<sup>-/-</sup> mice**

81 The first question we asked here was whether CCK is involved in trace fear memory formation.  
82 We studied transgenic CCK<sup>-/-</sup> mice (Cck-CreER, strain #012710, Jackson Laboratory), which  
83 lack CCK expression (X. Chen et al., 2019). We subjected CCK<sup>-/-</sup> and wildtype control (WT,  
84 C57BL/6) mice to trace fear conditioning using two training protocols: long trace interval and  
85 short trace interval training.

86 Trace fear conditioning was performed by collecting baseline readouts on pre-conditioning day,  
87 training with the appropriate CS-US pairings on conditioning days, and testing the conditioned  
88 fear responses on post-conditioning/testing day. In the long trace protocol, mice sequentially  
89 received a 10-second pure tone (as the CS), a 20-second gap (trace interval), and a 0.5-second  
90 foot shock (as the US) ([Figure 1a](#)). We calculated the percentage of time frames where mice  
91 displayed a freezing response as the measure of fear memory. Freezing percentages were  
92 compared before (baseline) and after (post-training) trace fear conditioning as well as before  
93 ([Figure 1b](#)) and after ([Figure 1c](#)) presentation of the CS. At baseline, CCK<sup>-/-</sup> (N = 10) and WT  
94 (N = 14) mice showed similarly low freezing percentages both before ([Figure 1b](#)) and after  
95 ([Figure 1c](#)) the CS ([Figure 1b](#), two-way repeated-measures analysis of variance [RM ANOVA],  
96 significant interaction,  $F [1,22] = 4.65$ ,  $P < 0.05$ ; pairwise comparison, WT vs. CCK<sup>-/-</sup> before  
97 CS,  $7.0\% \pm 1.1\%$  vs.  $5.9\% \pm 0.8\%$ ; Bonferroni test,  $P > 0.05$ ; [Figure 1c](#), two-way RM ANOVA],  
98 significant interaction,  $F [1,22] = 13.87$ ,  $P < 0.05$ ; pairwise comparison, WT vs. CCK<sup>-/-</sup> after  
99 CS,  $9.9\% \pm 1.6\%$  vs.  $9.6\% \pm 1.5\%$ , Bonferroni test,  $P > 0.05$ ). After conditioning, CCK<sup>-/-</sup> mice

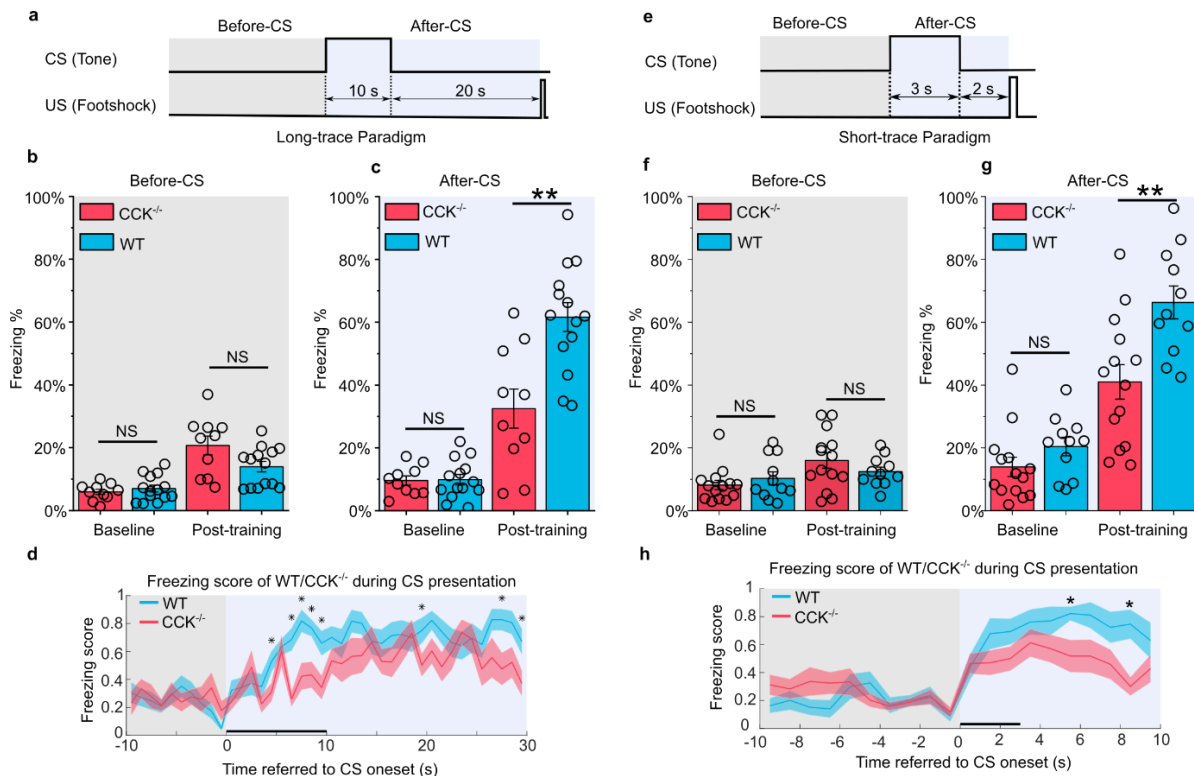


**Figure 1. Trace fear memory formation deficit in  $CCK^{-/-}$  mice.**

(a) Schematic diagram of the fear conditioning paradigm with a long trace interval of 20 s. Gray and light blue shadowed areas indicate the time frames before and after the onset of the CS (Before CS, After CS). CS, conditioned stimulus; US, unconditioned stimulus.

(b–c) Freezing percentages before (b) and after (c) the CS. Freezing percentages were recorded at baseline on the pre-conditioning day and post-training on the post-conditioning day. WT, wildtype,  $N = 14$ ;  $CCK^{-/-}$ , CCK-knockout,  $N = 10$ .  $*P < 0.05$ ;  $**P < 0.01$ ;  $***P < 0.001$ ; NS, not significant. Statistical significance was determined by two-way RM ANOVA with Bonferroni post-hoc pairwise test. RM ANOVA, repeated measures analysis of variance.

(d) Freezing score plot of the two groups of mice during the testing session. Solid lines indicate the mean value, and shadowed areas indicate the SEM. The black bar indicates the presence of the CS from 0 s to 10 s.  $*P < 0.05$ ; two-sample t-test; SEM, standard error of the mean.

(e) Schematic diagram of the fear conditioning paradigm with a short trace interval of 2 s. (f–g) Freezing percentages before (f) and after (g) the CS. WT,  $N = 11$ ;  $CCK^{-/-}$ ,  $N = 14$ .

(h) Freezing score plot of the two groups of mice during the testing session. The black bar indicates the presence of the CS from 0 s to 3 s.  $*P < 0.05$ ; two-sample t-test.

100 showed significantly lower freezing percentages ( $32.5\% \pm 6.2\%$ ) than WT mice after receiving  
 101 the CS ( $61.6\% \pm 4.6\%$ , pairwise comparison,  $P < 0.01$ ), indicating poor performance in  
 102 associating the CS with the US (Figure 1c, Movie S1, S2). This effect was not due to elevated  
 103 basal freezing levels caused by training in WT animals (Figure 1b). Instead, we found that  
 104  $CCK^{-/-}$  mice ( $20.7\% \pm 3.0\%$ ) had slightly higher freezing percentages than WT mice ( $14.0\% \pm$   
 105  $1.7\%$ ) in the absence of the CS (pairwise comparison,  $P > 0.05$ ). Together, these results suggest  
 106 that trace fear conditioning results in elevated conditioned freezing percentages in WT mice,  
 107 which are primarily elicited by the CS, and that loss of CCK impairs the freezing response to

108 the CS. Furthermore, we defined an empirical threshold of moving velocity and converted the  
109 moving velocity to a binary freezing score plot, in which value 1 represents active status, and  
110 value 0 represents freezing status (see [Methods](#)). Using this method, we were able to assess the  
111 freezing response of the animal as it occurred during the CS presentation. Again, we found that  
112 WT mice obtained higher average freezing scores than CCK<sup>-/-</sup> mice during the presentation of  
113 the CS ([Figure 1d](#), \* $P < 0.05$ , two-sample t-test).

114 In addition to the long trace interval, we also investigated freezing responses of mice during a  
115 short trace fear conditioning paradigm. Mice were presented a 3-second CS followed by a 2-  
116 second trace interval and a 0.5-second electrical foot shock ([Figure 1e](#)). Before training, WT  
117 (N = 11) and CCK<sup>-/-</sup> (N = 14) mice showed similarly low freezing percentages both before  
118 ([Figure 1f](#)) and after ([Figure 1g](#)) presentation of the CS ([Figure 1g](#), two-way RM ANOVA,  
119 significant interaction,  $F [1,23] = 4.85$ ,  $P < 0.05$ ; pairwise comparison, WT vs. CCK<sup>-/-</sup> in the  
120 baseline session,  $20.4\% \pm 2.9\%$  vs.  $13.9\% \pm 3.1\%$ ,  $P > 0.05$ ; [Figure 1f](#), two-way RM ANOVA,  
121 interaction not significant,  $F [1,23] = 1.8$ ,  $P = 0.19 > 0.05$ ; pairwise comparison, WT vs. CCK<sup>-/-</sup>  
122 in the baseline session,  $10.3\% \pm 2.1\%$  vs.  $8.2\% \pm 1.5\%$ ,  $P > 0.05$ ). Consistent with results  
123 from the long trace paradigm, CCK<sup>-/-</sup> mice showed an impaired freezing response ( $41.0\% \pm$   
124  $5.5\%$ ) to the CS after training compared to WT mice ( $66.3\% \pm 5.2\%$ , pairwise comparison,  $P$   
125  $< 0.01$ , [Figure 1g](#), [Movie S3](#), [S4](#)). Additionally, we observed no significant difference between  
126 fear conditioned WT and CCK<sup>-/-</sup> mice prior to the presentation of the CS ([Figure 1f](#), pairwise  
127 comparison, WT vs. CCK<sup>-/-</sup> in the post-training session,  $12.4\% \pm 1.4\%$  vs.  $16.0\% \pm 2.4\%$ ,  $P >$   
128  $0.05$ ). Finally, we found significant differences in freezing scores between WT and CCK<sup>-/-</sup> mice  
129 when presented the CS ([Figure 1h](#), \* $P < 0.05$ , two-sample t-test).

130 We conducted the innate hearing and fear expression examinations to rule out a potential  
131 inherent deficit derived from genome editing in CCK<sup>-/-</sup> transgenic mice. To evaluate hearing,  
132 we recorded the open-field auditory brainstem response (ABR) in anesthetized animals. We  
133 observed five peaks in both WT and CCK<sup>-/-</sup> mice at sound intensities above 50 dB of sound  
134 pressure level (dB SPL) ([Figure S1b](#)), and we did not observe any remarkable differences  
135 between the waveforms. Compared to WT mice, CCK<sup>-/-</sup> mice had better hearing ( $40.0 \pm 1.2$  dB  
136 in CCK<sup>-/-</sup> mice, N = 15, vs.  $47.3 \pm 2.1$  dB in WT mice, N = 11, two-sample t-test,  $P < 0.01$ ,  
137 [Figure S1c](#)). Thus, auditory perception does not account for the deficient trace fear memory  
138 formation of CCK<sup>-/-</sup> mice.

139 As fear expression is the behavioral output of fear conditioning, we wondered if CCK<sup>-/-</sup> mice  
140 suffered from a deficit in fear expression, which is observed in Klüver-Bucy syndrome and  
141 other diseases (Lilly et al., 1983). To test whether the CCK<sup>-/-</sup> mice have a deficit in fear  
142 expression, we presented a loud (90 dB SPL) white noise and quantified sound-driven innate  
143 freezing. We found no statistical difference between WT ( $46.1\% \pm 5.5\%$ , N = 11) and CCK<sup>-/-</sup>  
144 mice ( $46.5\% \pm 6.6\%$ , N = 14, two-sample t-Test,  $P > 0.05$ , [Figure S1d](#)), indicating that CCK<sup>-/-</sup>  
145 mice can express passive defensive behaviors such as freezing. Thus, the deficient trace fear  
146 memory formation of CCK<sup>-/-</sup> is not due to a deficit in fear expression and may be due to a  
147 deficit in establishing an association between the CS and the US.

148 In summary, CCK<sup>-/-</sup> mice display deficient trace fear memory formations in both short and long  
149 trace models that are not caused by inherent abnormalities in hearing or fear expression.

### 150 **Deficient neural plasticity in the LA of CCK<sup>-/-</sup> mice**

151 As neural plasticity in the LA is widely regarded as the basis of fear memory formation (Kim  
152 & Cho, 2017; LeDoux, 2000; Nabavi et al., 2014; Rogan et al., 1997), we examined LTP in the  
153 LA of WT and CCK<sup>-/-</sup> mice by *in vivo* recording ([Figure 2a](#)). First, we successfully recorded  
154 the auditory evoked potential (AEP) in the LA of anesthetized WT and CCK<sup>-/-</sup> mice ([Figure](#)

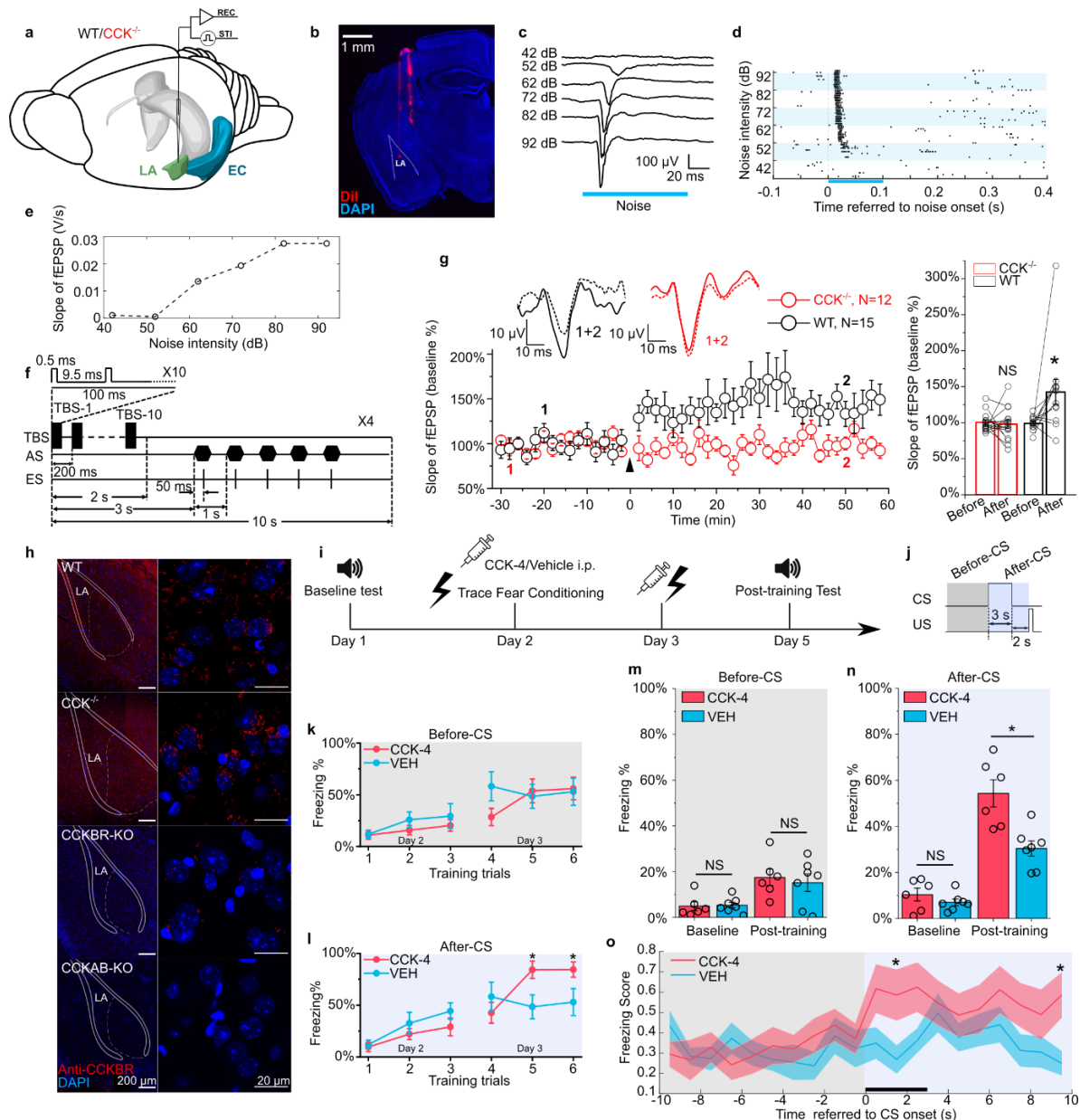


**Figure 2. Neural plasticity deficit in the LA of CCK<sup>-/-</sup> mice and the rescuing effect of exogenous CCK.**

(a) Schematic diagram of *in vivo* recording in the LA. EC, entorhinal cortex; LA, lateral amygdala. STI, stimulation. REC, recording.

(b) Post-hoc verification of electrode tracks and recording area.

(c) Representative AEP traces in response to different levels of noise stimulus. AEP, auditory evoked potential.

(d) Representative traces of multiunit spikes to different levels of noise stimulus.

(e) Representative input/output (I/O) curve of the slope of AEP versus noise intensity. fEPSP, field excitatory postsynaptic potential.

(f) Schematic diagram of the pairing protocol to induce LTP of AEP via theta-burst stimulation (TBS). LTP, long term potentiation; ES, electrical stimulation; AS, auditory stimulation.

(g) Time course plot of the normalized AEP slope during LTP. The WT group is indicated in black, and the CCK<sup>-/-</sup> group is indicated in red. Representative traces of the AEP before (dotted line) and after (solid line) TBS are shown in inset panels for both groups. The average normalized slopes 10 min before pairing (-10-0 min, before) and 10 min after pairing (50-60 min, after) in the two groups of mice are shown on the right. \*\*\* $P < 0.05$ ; two-way RM ANOVA with Bonferroni post-hoc pairwise test; RM ANOVA, repeated measures analysis of variance; NS, not significant.

(h) Immunofluorescent staining of CCK B receptor (CCKBR) in brain slices from WT, CCK<sup>-/-</sup>, CCKBR-KO, and CCKAB-KO mice. Magnified images are shown on the right. CCKBR-KO, CCK B receptor knock-out mouse; CCKAB-KO, CCK A receptor and B receptor double knock-out mouse.

(i) Experimental timeline for (j-o).

(j) Schematic diagram of the CS-US presentation. Gray and light blue shadowed areas indicate the time frames before and after CS presentation (Before-CS, After-CS).

(k-l) Freezing percentages before (k) and after (l) the CS during fear conditioning training on training day. Animals underwent six trials during a 2-day training (day 2 and 3). CCK-4, N = 6; VEH, N = 6; \* $P < 0.05$ ; two-sample t-test.

(m-n) Freezing percentages before (m) and after (n) the CS on the pre-training day (baseline) and the post-training day. CCK-4, N = 6; VEH, N = 6; \* $P < 0.05$ ; NS, not significant; two-way RM ANOVA with Bonferroni post-hoc pairwise test; RM ANOVA, repeated measures analysis of variance.

(o) Freezing score plot of the two groups of mice during the testing session on day 5. Solid lines indicate the mean value, and shadowed areas indicate the SEM. The black bar indicates the presence of the CS from 0 s to 3 s. \* $P < 0.05$ ; two-sample t-test; SEM, standard error of the mean.

155 [2b-e](#)). Then, we used theta-burst electrical stimulation (TBS) to induce LTP of AEP (AEP-  
156 LTP) ([Figure 2f](#)). Interestingly, AEP-LTP was effectively induced in WT mice (N = 15) but  
157 was not in CCK<sup>-/-</sup> mice (N = 12). WT mice demonstrated remarkable potentiation ([Figure 2g](#),  
158 two-way RM ANOVA, significant interaction,  $F [1,25] = 6.8$ ,  $P = 0.015 < 0.05$ ; pairwise  
159 comparison, after vs. before induction,  $142.7\% \pm 17.5\%$  vs.  $99.1\% \pm 2.8\%$ ,  $P = 0.011 < 0.05$ ),  
160 whereas CCK<sup>-/-</sup> mice showed no potentiation (pairwise comparison, after vs. before induction,  
161  $98.0\% \pm 5.8\%$  vs.  $100.6\% \pm 3.4\%$ ,  $P > 0.05$ ). These results suggest that CCK<sup>-/-</sup> mice have a  
162 deficit in neural plasticity in the LA that may contribute to their reduced response to trace fear  
163 conditioning.

#### 164 **Stimulation of CCKBR rescues the formation of trace fear memory in CCK<sup>-/-</sup> mice**

165 Although the translation and release of CCK are disrupted in CCK<sup>-/-</sup> mice, we found that the  
166 predominant CCK receptor, CCKBR, was expressed normally in both WT and CCK<sup>-/-</sup> mice  
167 ([Figure 2h](#)). Therefore, we hypothesized that exogenous stimulation of CCKBR might rescue  
168 trace fear memory deficits in CCK<sup>-/-</sup> mice. CCKBR can be stimulated by several agonists,  
169 including CCK octapeptide sulfated (CCK-8s) and CCK tetrapeptide (CCK-4). As CCK-8s is  
170 a potent agonist of both CCKAR and CCKBR, we selected CCK-4, which is a preferred  
171 CCKBR agonist (Berna et al., 2007). To monitor CCK signaling *in vivo*, we expressed a G  
172 protein-coupled receptor (GPCR)-activation-based CCK sensor (GRAB<sub>CCK</sub>, AAV-hSyn-  
173 CCK2.0) in the LA of CCK<sup>-/-</sup> mice (Jing et al., 2019). Using this model, binding of the GPCR  
174 CCKBR with endogenous or exogenous CCK results in increased fluorescence intensity, which  
175 we measured by fiber photometry in the LA ([Figure S2a](#)). We first confirmed that

176 intraperitoneal (i.p.) administration of CCK-4 permeated the blood-brain-barrier (BBB) and  
177 activated the CCK2.0 sensor. Moreover, we demonstrated that administration of CCK-4  
178 evoked a clear and long-term increase in the fluorescent signal ([Figure S2b](#)). Together, these  
179 data verify that CCK-4 passes through the BBB and binds with CCKBR in the LA.

180 After validating our model, we conducted short trace fear conditioning in CCK<sup>-/-</sup> mice on two  
181 consecutive days just after intraperitoneal administration of CCK-4 or the corresponding  
182 vehicle (VEH) ([Figure 2i-j](#)). We collected data during the two conditioning days to monitor  
183 the learning curve of mice as conditioning progressed. The learning curves were plotted as the  
184 freezing percentages of CCK-4- or VEH-treated CCK<sup>-/-</sup> mice during the six training trials  
185 ([Figure 2k-l](#)). During the first three trials on the first conditioning day and even in the fourth  
186 trial on the second conditioning day, we did not observe any statistical differences between the  
187 two groups. During the fifth and sixth training trials conducted on the second conditioning day,  
188 we found that CCK-4-treated mice had significantly higher freezing levels than VEH-treated  
189 mice ([Figure 2l](#), 84.2% ± 8.4% in the CCK-4 group [N = 6] vs. 48.4% ± 11.5% in the VEH  
190 group [N = 7] in the fifth trial; 84.4% ± 7.3% in the CCK-4 group vs. 52.9% ± 13.0% in the  
191 VEH group in the sixth trial, two-sample t-test, both  $P < 0.05$ ). In support of this evidence, we  
192 did not find a statistical difference between the two groups prior to CS presentation during the  
193 fifth or sixth trials ([Figure 2k](#), 53.8% ± 11.5% in the CCK-4 group vs. 52.5% ± 11.8% in the  
194 VEH group in the fifth trial; 56.0% ± 10.8% in the CCK-4 group vs. 47.8% ± 11.8% in the  
195 VEH group in the sixth trial, two-sample t-test, both  $P > 0.05$ ). Together, these data suggest  
196 that mice in the CCK-4- and VEH-treated groups showed similar baseline freezing levels and  
197 that CCK-4 treatment improved trace fear conditioning learning responses in CCK<sup>-/-</sup> mice.

198 We went on to assess the conditioned fear response in CCK-4- and VEH-treated CCK<sup>-/-</sup> mice  
199 two days after training in comparison to fear responses at baseline prior to training ([Figure 2m-](#)  
200 [n](#)). We found that CCK4-treated mice showed remarkably higher freezing levels than VEH-  
201 treated mice post-training, whereas no significant difference was detected at baseline ([Figure](#)  
202 [2n](#), two-way RM ANOVA, significant interaction,  $F [1,11] = 6.40, P = 0.028 < 0.05$ ; pairwise  
203 comparison, CCK-4 vs. VEH at baseline, 10.4% ± 2.8% vs. 7.0% ± 1.4%,  $P > 0.05$ ; CCK-4 vs.  
204 VEH post-training, 54.3% ± 5.9% vs. 30.4% ± 3.3%,  $P < 0.05$ ; [Movie S5, S6](#)). There was no  
205 statistical difference between the two groups before the presentation of the CS ([Figure 2m](#),  
206 two-way RM ANOVA, the main effect of drug application [CCK-4 vs. VEH] on freezing  
207 percentage was not significant,  $F [1,11] = 0.15, P = 0.70$ ). Additionally, CCK-4-treated mice  
208 had significantly higher freezing scores than VEH-treated mice ([Figure 2o](#)). These results  
209 indicate that CCK-4 treatment effectively improved learning response to trace fear conditioning  
210 in CCK<sup>-/-</sup> mice. Moreover, this rescue was not an artifact caused by reduced locomotion after  
211 drug application and fear conditioning training, as there was no difference between the two  
212 groups in the freezing percentage prior to presentation of the CS ([Figure 2m](#)). Therefore, the  
213 exogenous application of a CCKBR agonist activated endogenous CCKBR and improved the  
214 fear memory formation of CCK<sup>-/-</sup> mice after trace fear conditioning.

### 215 **CCK neurons in the EC are critical for the formation of the trace fear memory**

216 We next examined the source of endogenous CCK that signals to the LA. We injected a potent  
217 retrograde neuronal tracer Cholera Toxin Subunit B (CTB) conjugated to a fluorescent tag  
218 Alexa-647 (CTB-647) into the LA and dissected the upstream anatomical brain regions that  
219 project to the LA ([Figure 3a](#)). In addition to regions that are canonically involved in fear  
220 circuitry, including the auditory cortex (AC) and the medial geniculate body (MGB), we found  
221 that EC was also densely labeled with retrograde CTB-647, suggesting that the EC is connected  
222 with the LA ([Figure 3b-e](#)). We next injected a Cre-dependent retrograde AAV (retroAAV-  
223 hSyn-FLEX-jGcamp7s) into the LA of CCK-ires-Cre (CCK-Cre) mice to label CCK-positive



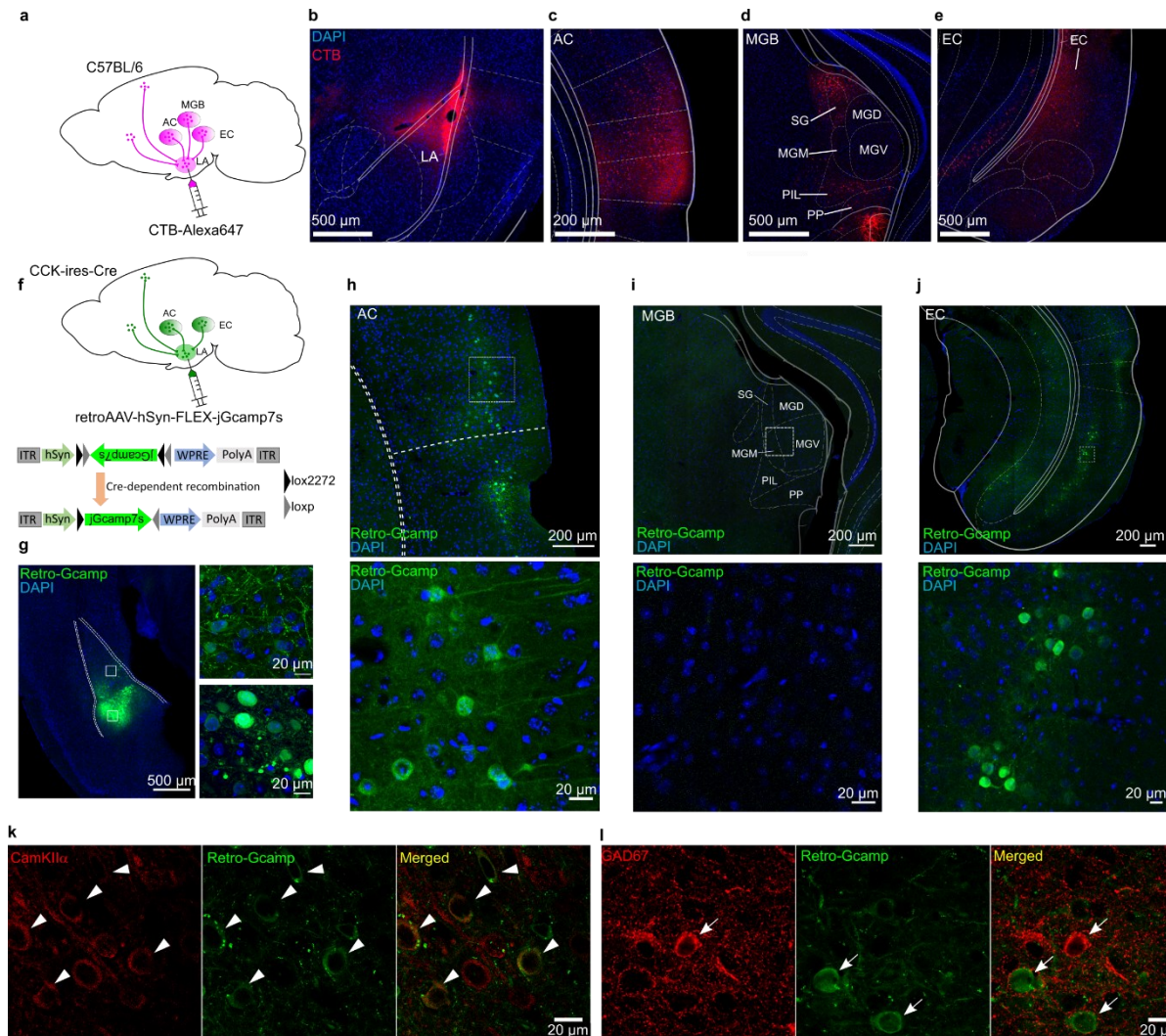


**Figure 3. Dissection of inputs of the LA with retrograde tracer and virus.**

(a) Schematic diagram of retrograde tracing with Alexa647-conjugated cholera toxin subunit B (CTB).

(b–e) Representative fluorescent images of the injection site of the CTB tracer (b), the canonical upstream regions, including the auditory cortex (c) and the auditory thalamus (d), and the non-canonical entorhinal cortex (e). AC, auditory cortex; MGB, medial geniculate body; SG, supragenulate thalamic nucleus; MGM, medial MGB; PIL, posterior intralaminar thalamic nucleus; PP, peripeduncular nucleus; EC, entorhinal cortex.

(f) Schematic diagram of cell type-specific retrograde tracing with Cre-dependent retrograde AAV (retroAAV-hSyn-FLEX-jGcamp7s).

(g) Verification of the injection site in the LA. Magnified images are shown in insets on the right. Retro-Gcamp, retrograde jGcamp7s signal.

(h–j) Retrograde signals in the AC (h), MGB (i), and EC (j). Magnified images are shown in the bottom insets.

(k–l) Co-immunofluorescent staining of retrograde tracing of the LA with either the excitatory neuronal marker CamKII $\alpha$  (k) or the inhibitory neuronal marker GAD67 (l).

224 neurons that project into the LA, to further confirm the above observation ([Figure 3f-g](#)). In  
225 CCK-ires-Cre mouse line, Cre expression was restricted to the CCK-expressing neurons, where  
226 the Cre-mediated recombination took place and the Cre-dependent green, fluorescent protein  
227 jGcamp7s was expressed ([Figure 3f](#)). Fluorescent signal was detected in the AC and the EC,  
228 but not in the MGB ([Figure 3h-j](#)), which suggests that CCK may originate from these two brain  
229 regions during trace fear memory formation. Immunofluorescent staining revealed that most  
230 CCK-positive neurons in the EC that project to the LA are glutamatergic ([Figure 3k-l](#)), which  
231 is consistent with our previous findings in CCK-positive neurons in the EC (X. Chen et al.,  
232 2019).

233 Interestingly, the EC is involved in the formation of trace fear memory but is not a component  
234 of canonical delay fear memory (Esclassan et al., 2009). This selectivity suggests that the EC  
235 may be a component of the neural circuit underlying trace fear memory formation. To evaluate  
236 a requirement for the EC in trace fear memory, we utilized a Designer Receptors Exclusively  
237 Activated by Designer Drugs (DREADD) system to silence EC neurons (Armbruster et al.,  
238 2007). Specifically, the inhibitory receptor hM4Di was expressed in the EC of WT mice  
239 ([Figure 4a](#)) and was activated by administration of the designer drug clozapine (CLZ).  
240 Activation of hM4Di by CLZ induces membrane hyperpolarization, effectively silencing  
241 neurons. We verified EC neuron silencing by *in vivo* electrophysiological recording ([Figure](#)  
242 [4b-d](#) and [Figure S3](#)). We found that a low dose of CLZ (0.5 mg/kg) effectively suppressed  
243 both instant and long-term neuronal firing. Of note, we used CLZ instead of the canonical  
244 DREADD ligand clozapine-N-oxide (CNO). A recent study identified CLZ as the active  
245 metabolite of CNO (Gomez et al., 2017), and CLZ more effectively penetrates the BBB and  
246 binds with DREADD receptors compared to CNO. As a result, a much lower dose of CLZ can  
247 elicit similar behavioral effects as higher doses of CNO (Gomez et al., 2017). Therefore, we  
248 used a low dose of CLZ (0.5 mg/kg) in our experiments.

249 Six weeks after injection of AAV9-hSyn-hM4Di-EGFP or AAV9-hSyn-EGFP, we  
250 administered CLZ by intraperitoneal injection and conducted short trace fear conditioning 30  
251 min later. We repeated the CLZ treatment and trace fear conditioning the following day and  
252 tested conditioned fear responses two days after that. As expected, mice expressing hM4Di  
253 (hM4Di, N = 7) showed significantly lower freezing percentages in response to the CS than  
254 those expressing the control virus (EGFP, N = 7) post-training ([Figure 4f](#), two-way RM  
255 ANOVA, significant interaction,  $F [1,12] = 7.42$ ,  $P = 0.018 < 0.05$ ; EGFP vs. hM4Di post-  
256 training,  $68.1\% \pm 10.0\%$  vs.  $39.0\% \pm 5.7\%$ ,  $P = 0.035 < 0.05$ ; [Movie S7, S8](#)). No significant  
257 differences were observed between the two groups at baseline ([Figure 4f](#), pairwise comparison,  
258 EGFP vs. hM4Di at baseline,  $12.0\% \pm 3.1\%$  vs.  $15.0\% \pm 3.3\%$ ,  $P > 0.05$ ) or prior to the CS  
259 ([Figure 4e](#), two-way RM ANOVA, interaction not significant,  $F [1, 12] = 0.05$ ,  $P = 0.82 > 0.05$ ;  
260 pairwise comparison, EGFP vs. hM4Di post-training,  $16.0\% \pm 3.8\%$  vs.  $16.4\% \pm 4.7\%$ ,  $P >$   
261  $0.05$ ).

262 As we have shown that CCK-positive neural projections extend from the EC to the LA, we  
263 transfected CCK-expressing neurons in the EC with a Cre-dependent hM4Di in CCK-Cre mice  
264 ([Figure 4h-j](#)). These mice received an i.p. injection of CLZ (N = 10) or VEH (N = 10) prior to  
265 long trace fear conditioning. After training, mice injected with CLZ showed significantly lower  
266 freezing percentages than those injected with the VEH, whereas no statistical differences were  
267 observed at baseline or prior to the CS ([Figure 4l](#), two-way RM ANOVA, significant  
268 interaction,  $F [1,18] = 5.90$ ,  $P = 0.026 < 0.05$ ; pairwise comparison, CLZ vs. VEH at baseline,  
269  $12.9\% \pm 1.7\%$  vs.  $14.2\% \pm 2.2\%$ ,  $P > 0.05$ ; CLZ vs. VEH post-training,  $48.4\% \pm 7.4\%$  vs.  $27.1\%$   
270  $\pm 3.7\%$ ,  $P = 0.017 < 0.05$ ; [Figure 4k](#), two-way RM ANOVA, interaction not significant,  $F [1,$   
271  $18] = 0.043$ ,  $P = 0.84 > 0.05$ ; pairwise comparison, CLZ vs VEH at baseline,  $10.2\% \pm 2.4$  vs.

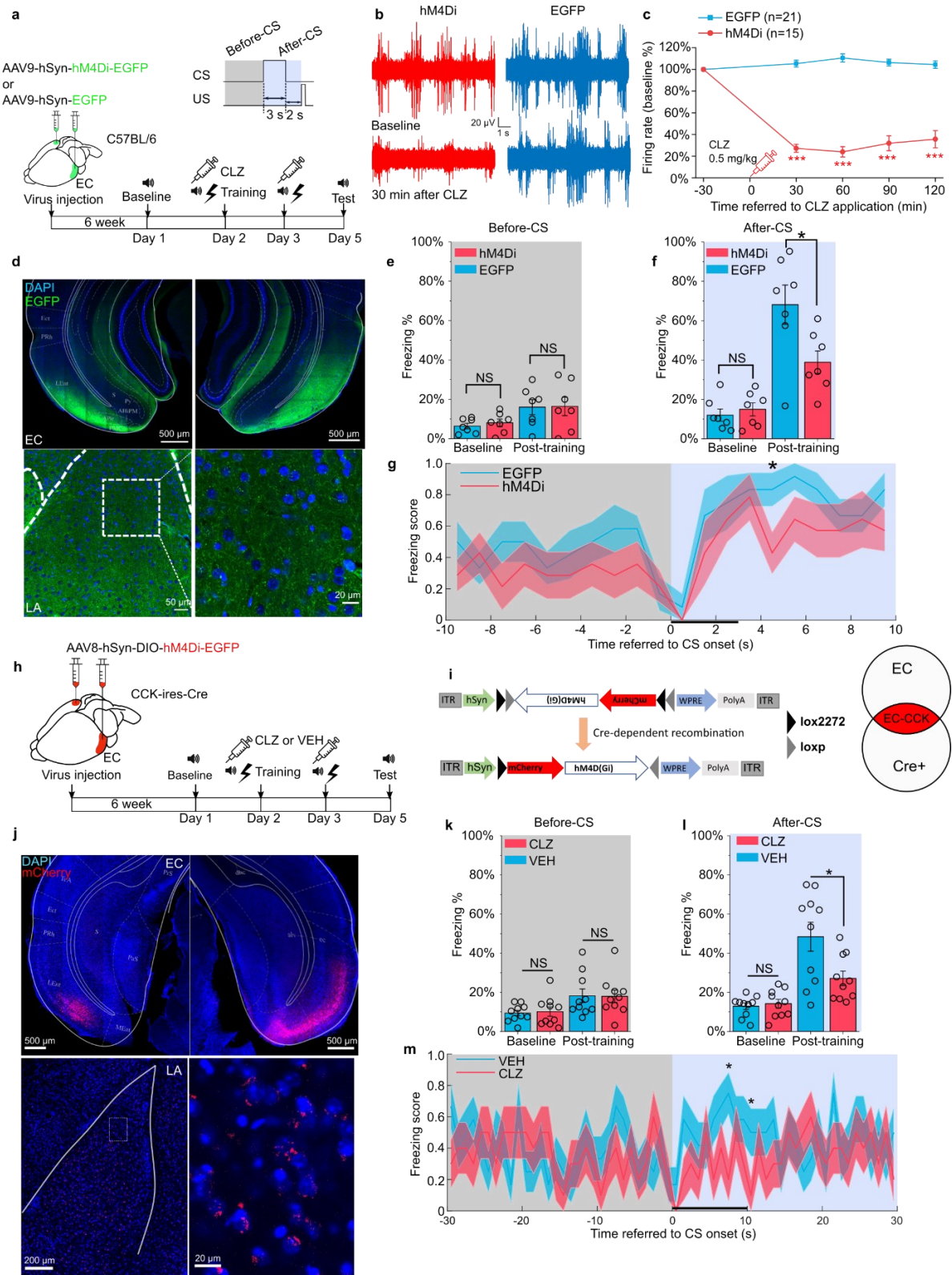


**Figure 4. Formation of trace fear memory is suppressed by chemogenetic inhibition of the EC and CCK-positive EC neurons.**

(a) Schematic diagram of trace fear conditioning and chemogenetic inhibition of the EC. EC, entorhinal cortex; hM4Di, inhibitory DREADD receptor; CLZ, clozapine.

(b) Representative traces of extracellular recording in the EC before and after systemic application of CLZ in hM4Di-expressing (red) and EGFP-expressing mice (blue).

(c) Normalized firing rate of the EC neurons before and after systemic CLZ application. \*\*\* $P < 0.001$ ; two-sample t-test.

(d) Verification of viral expression in the bilateral EC (top panel) and the EC-LA projection (bottom left panel). A magnified image of the EC-LA projection is shown in the bottom right inset.

(e–f) Freezing percentages before (e) and after (f) the CS during the testing session in hM4Di-expressing ( $N = 7$ ) or EGFP-expressing mice ( $N = 7$ ). \* $P < 0.05$ ; NS, not significant; two-way RM ANOVA with Bonferroni post-hoc pairwise test; RM ANOVA, repeated measures analysis of variance.

(g) Freezing score plot of hM4Di-expressing and EGFP-expressing mice during the testing session. Solid lines indicate the mean value, and shadowed areas indicate the SEM. The black bar indicates the presence of the CS from 0 s to 3 s. \* $P < 0.05$ ; two-sample t-test; SEM, standard error of the mean.

(h–i) Schematic diagrams of chemogenetic CCK inhibition in the EC. Cre-dependent hM4Di was expressed in CCK-Cre mice. After Cre-mediated recombination, CCK neurons in the EC were transfected with hM4Di.

(j) Verification of viral expression in the bilateral EC (top panel) and the EC-LA projection (bottom left panel). A magnified image of the EC-LA projection is shown in the bottom right inset.

(k–l) Freezing percentages before (k) and after (l) the CS during the testing session in mice treated with CLZ or vehicle (VEH). \* $P < 0.05$ ; NS, not significant; two-way RM ANOVA with Bonferroni post-hoc pairwise test.

(m) Freezing score plot of CLZ- and VEH-treated mice during the testing session. The black bar indicates the presence of the CS from 0 s to 10 s. \* $P < 0.05$ ; two-sample t-test; SEM, standard error of the mean.

272 9.4%  $\pm$  1.4%,  $P > 0.05$ ; CLZ vs. VEH post-training, 18.0%  $\pm$  3.2% vs. 18.3%  $\pm$  3.4%,  $P > 0.05$ ;  
273 [Movie S9, S10](#)). These results mirror those observed in CCK<sup>-/-</sup> mice and suggest that trace fear  
274 memory formation relies on intact and functional CCK-positive neurons in the EC.

### 275 **CCK-positive neuronal projections are predominant in the EC-LA pathway**

276 To further demonstrate that afferents to the amygdala originate from CCK-expressing neurons  
277 in the EC, we locally injected a Cre-dependent color-switching virus (AAV-CAG-DO-  
278 mCherry-DIO-EGFP) in the EC of CCK-Cre mice ( $N = 2$ ; [Figure 5a–b](#)). With this combination,  
279 CCK-positive neurons express EGFP, and CCK-negative neurons express mCherry (Saunders  
280 et al., 2012). We found that EGFP<sup>+</sup> (i.e., CCK<sup>+</sup>) neurons made up a slightly higher proportion  
281 of labeled neurons than mCherry<sup>+</sup> (i.e., CCK<sup>-</sup>) neurons ([Figure 5c–d](#), EGFP vs. mCherry, 58.9%  
282  $\pm$  4.8% vs. 38.6%  $\pm$  5.0%, one-way RM ANOVA, Wilks' Lambda = 0.58,  $F [1,6] = 4.34$ ,  $P =$   
283 0.0822  $> 0.05$ ). Interestingly, we found that CCK<sup>+</sup> neural projections from the EC to the LA  
284 were densely labeled with EGFP, whereas mCherry labeling of CCK<sup>-</sup> projections was  
285 dramatically weaker. Quantitative analysis revealed that the projection intensity of the  
286 EC<sup>CCK<sup>+</sup></sup>  $\rightarrow$  LA was 3-fold higher than the EC<sup>CCK<sup>-</sup></sup>  $\rightarrow$  LA (35.6%  $\pm$  9.5%). In other words, CCK-  
287 positive afferents constituted approximately 75% of total afferents from the EC to the LA  
288 ([Figure 5e–f](#)).

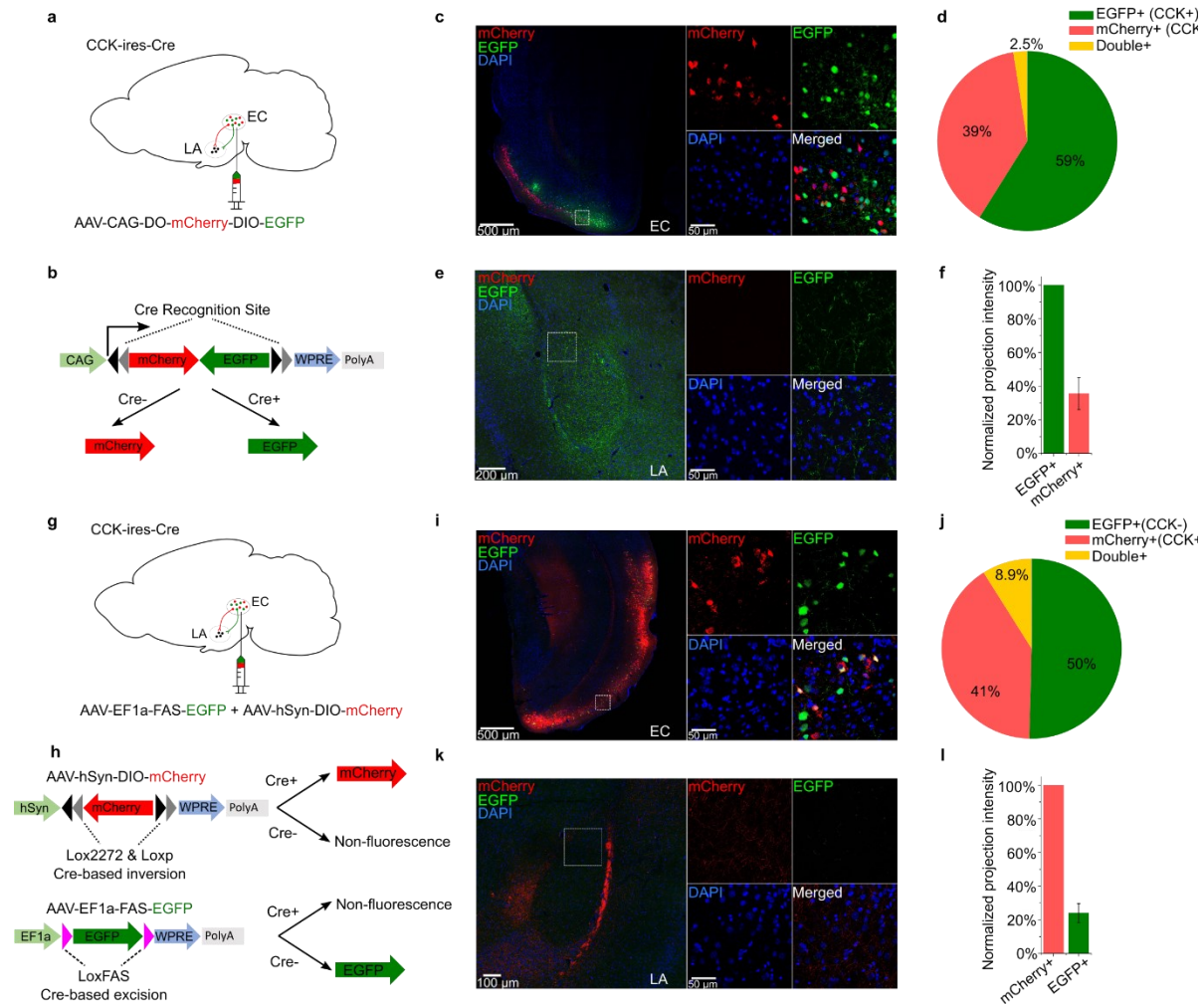


**Figure 5. CCK-expressing projections predominate in the EC-LA pathway.**

(a–b) Schematic diagram of Cre-dependent color-switch labeling in the EC-LA pathway. AAV-CAG-DO-mCherry-DIO-EGFP was injected in the EC. Using this labeling scheme, EGFP is expressed in CCK+ neurons, and mCherry is expressed in CCK– neurons.

(c–d) Visualization (c) and quantification (d) of viral expression in the EC. Representative immunofluorescent images in the EC 7 weeks after viral injection (c). Scale bar = 500 μm (left). Magnified images are shown in insets on the right. Scale bar = 50 μm. Percentages of EGFP+ (CCK+), mCherry+ (CCK–), and double-positive neurons (d). No statistical differences were observed.  $P = 0.08$ ; one-way RM ANOVA, repeated measures analysis of variance.

(e–f) Visualization (e) and quantification (f) of EGFP-expressing (CCK+) and mCherry-expressing (CCK–) afferents in the amygdala stemming from the EC. The fluorescent intensity of neuronal projections was normalized to the EGFP+ signal, which was approximately 3-fold stronger than the mCherry+ signal ( $35.6\% \pm 9.5\%$ ).

(g–h) Schematic diagram of Cre-dependent color-switch labeling in the EC-LA pathway. A mixture of AAV-hSyn-DIO-mCherry and AAV-EF1α-FAS-EGFP was injected in the EC. Using this labeling scheme, mCherry is expressed in CCK+ neurons, and EGFP is expressed in CCK– neurons.

(i–j) Visualization (i) and quantification (j) of viral expression in the EC. Representative immunofluorescent images in the EC 7 weeks after viral injection (c). Scale bar = 500  $\mu\text{m}$  (left). Magnified images are shown in insets on the right. Scale bar = 50  $\mu\text{m}$ . Percentages of mCherry+ (CCK+), EGFP+ (CCK-), and double-positive neurons (j). No statistical differences were observed.  $P = 0.55$ ; one-way RM ANOVA; Wilks' Lambda = 0.94;  $F(1,6) = 0.39$ .

(k–l) Visualization (k) and quantification (l) of EGFP-expressing (CCK+) and mCherry-expressing (CCK-) afferents in the amygdala stemming from the EC. The fluorescent intensity of neuronal projections was normalized to the mCherry+ signal, which was approximately 4-fold stronger than the EGFP+ signal ( $24.0\% \pm 5.6\%$ ).

289 To determine if the fluorescent reporter proteins interfered with projection strength, we  
290 inverted the color combination by combining two AAVs: AAV-hSyn-DIO-mCherry and AAV-  
291 EF1 $\alpha$ -FAS-EGFP (Saunders et al., 2012). These Cre-dependent AAVs were injected into the  
292 EC of CCK-Cre mice. In CCK-Cre mice, AAV-hSyn-DIO-mCherry induces Cre-ON mCherry  
293 expression in CCK+ neurons, and AAV-EF1 $\alpha$ -FAS-EGFP induces Cre-OFF EGFP expression  
294 in CCK- neurons (Figure 5g–h). With the mixed AAVs, we labeled approximately 50% CCK-  
295 EGFP+ neurons, 41% CCK+ mCherry+ neurons, and 8.9% double-positive neurons (Figure  
296 5i–j). The higher percentage of double-positive neurons present in this system indicates a  
297 higher probability of off-target effects compared to the previous color-switching AAV ( $8.9\%$   
298  $\pm 2.7\%$  vs.  $2.5\% \pm 1.1\%$ ). Consistent with the previous color-switching AAV, we observed that  
299 CCK+ (mCherry+) projections were predominant. Specifically, the intensity of the  
300 EC<sup>CCK+</sup>→LA was approximately 4-fold higher than the EC<sup>CCK-</sup>→LA ( $24.0\% \pm 5.6\%$ ).  
301 Altogether, our results suggest that the EC<sup>CCK+</sup>→LA is the predominant subpopulation of  
302 projections, and that these projections are of functional significance in the EC-LA pathway.

### 303 CCK-positive neural projections from the EC to the LA enable neural plasticity and 304 modulate trace fear memory formation

305 Finally, we asked whether CCK-positive projections from the EC modulate neural plasticity in  
306 the LA. First, we expressed a Cre-dependent high frequency-responsive channelrhodopsin  
307 (ChR2) variant E123T (ChETA) under control of the universal EF1 $\alpha$  promoter in CCK-Cre  
308 mice (Figure 6a). Then, we implanted optic fibers targeting the LA to illuminate EC<sup>CCK+</sup>→LA  
309 projections and electrodes to conduct *in vivo* electrophysiological recording as before (Figure  
310 6b). Post-hoc anatomical analysis confirmed the distribution of ChETA in the EC-LA axon  
311 terminals (Figure 6c). These CCK+ projections were innervated with postsynaptic CCKBR  
312 (Figure 6d), suggesting that CCK+ projections from the EC effectively activated CCKBR in  
313 the LA. Finally, we recorded auditory evoked potential (AEP) and visual evoked potential  
314 (VEP) in the LA of anesthetized mice (Figure 6e–g). Although AEP and VEP had similar  
315 waveforms, the latency of AEP was much shorter than VEP (Figure 6e–f, peak latency:  $38.9 \pm$   
316  $3.2$  ms for AEP,  $N = 13$ , vs.  $89.5 \pm 3.1$  ms for VEP,  $N = 11$ , two-sample t-test,  $P < 0.001$ ). This  
317 observation implies that input pathways other than the canonical thalamo-cortico-amygdala  
318 and thalamo-amygdala projections regulate the transmission of visual cues. We applied high-  
319 frequency-laser-stimulation (HFLS, Figure 6h) of the EC-LA axons before the auditory  
320 stimulus (AS) to trigger AEP-LTP in the LA. After induction, the AEP slope in the ChETA-  
321 expressing group ( $n = 10$ ) increased significantly, whereas the VEP slope did not change  
322 (Figure 6i–j, two-way RM ANOVA, significant interaction,  $F[1,9] = 14.46$ ,  $P = 0.0042 < 0.01$ ;  
323 pairwise comparison, AEP before vs. after pairing,  $97.8\% \pm 5.5\%$  vs.  $187.6\% \pm 15.6\%$ ,  $P <$   
324  $0.001$ ; VEP before vs. after pairing,  $96.3\% \pm 4.9\%$  vs.  $120.7\% \pm 9.1\%$ ,  $P = 0.67$ ). Additionally,  
325 we injected a non-opsin expressing control AAV (AAV-EF1 $\alpha$ -DIO-EYFP,  $n = 20$ ) and the

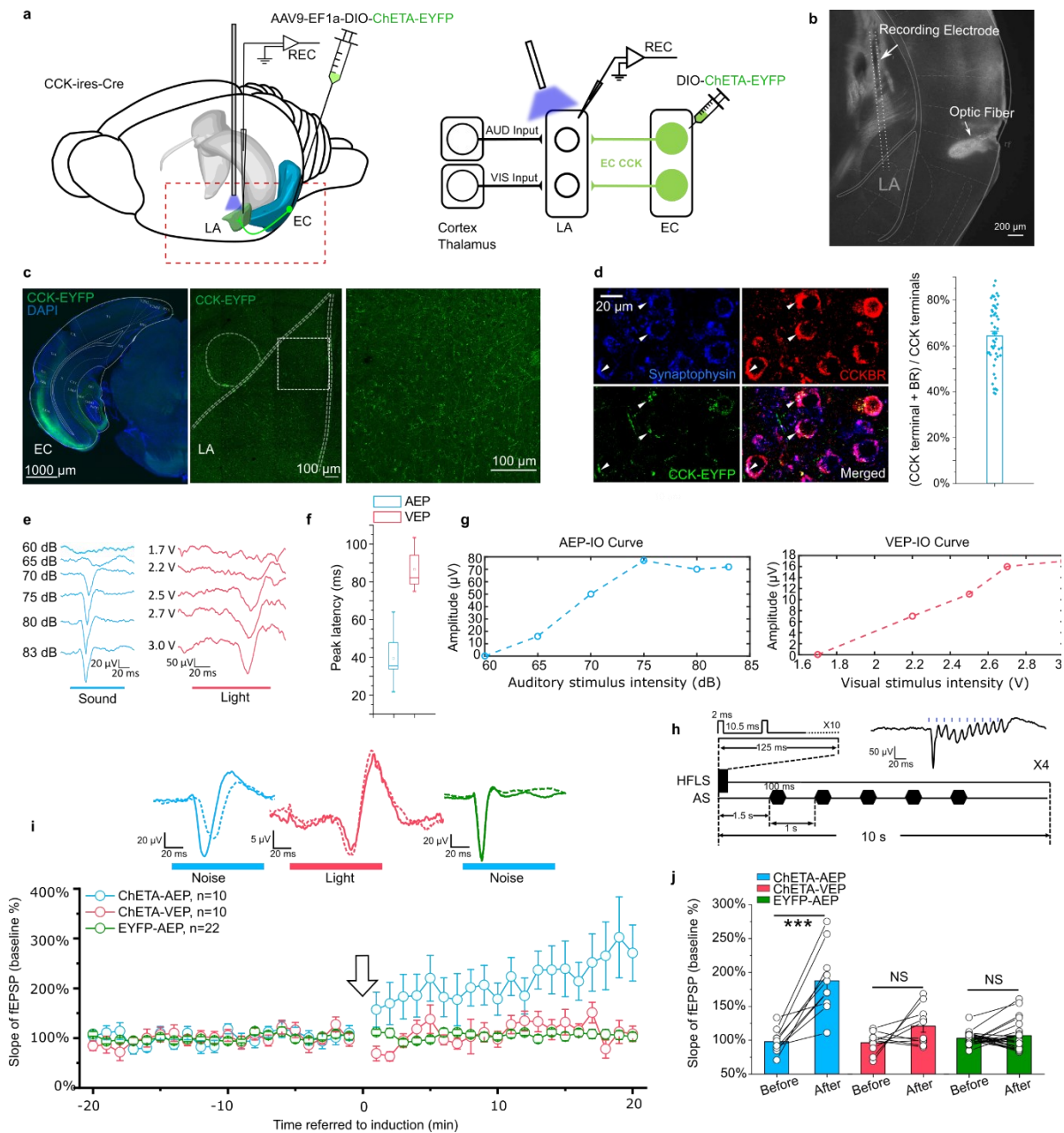


**Figure 6. High frequency activation of the EC<sup>CCK+</sup>→LA pathway induces LTP of AEP in the LA.**

(a) Schematic diagram of the experiment. The Cre-dependent high frequency-responsive opsin ChETA was expressed in the EC of CCK-Cre mice. Electrodes were inserted into the LA, and blue light was used to illuminate the recording area. The red rectangle in the left panel is magnified in the right panel to illustrate the neural pathways that are recruited during recording. AUD, auditory stimulus; VIS, visual stimulus; LA, lateral amygdala; EC, entorhinal cortex; REC, recording.

(b) Post-hoc verification of the electrode tracks and optic fiber placement.

(c) Post-hoc verification of viral expression in the EC (left) and in CCK-positive projections in the LA (middle). A magnified image is shown in the right panel and corresponds to the boxed area of the middle panel.

- (d) Co-immunofluorescent staining of the CCK-positive fiber (EYFP), the axon terminal (synaptophysin), and CCKBR in the LA. The white arrowhead indicates a triple-positive neural terminal. Quantification of the CCK and CCKBR double-positive neural terminals out of all CCK-positive terminals (right).
- (e) Representative traces of auditory evoked potential (AEP) and visual evoked potential (VEP) at different sound and light intensities.
- (f) AEP and VEP peak latency.
- (g) Representative input/output (IO) curves for AEP (left) and VEP (right).
- (h) Detailed pairing protocol to induce LTP. Representative averaged fEPSP trace evoked by HFLS is shown in the inset. HFLS, high frequency laser stimulation; AS, auditory stimulation.
- (i) Time course plot of the normalized slope of AEP and VEP during LTP. The arrow indicates the application of LTP induction. Representative traces of averaged AEP/VEP before (-10-0 min, dotted line) and after (10-20 min, solid line) induction from the three groups are shown in the top insets.
- (j) The average normalized slopes 10 min before pairing (-10-0 min, before) and 10 min after pairing (10-20 min, after) in the three groups. \*\*\* $P < 0.001$ ; two-way RM ANOVA with Bonferroni post-hoc pairwise test; RM ANOVA, repeated measures analysis of variance; NS, not significant.

326 AEP-LTP was not induced with the same protocol (two-way RM ANOVA between CHETA  
327 and EYFP,  $F [1,30] = 46.65$ ,  $P < 0.001$ ; pairwise comparison, before vs. after pairing in the  
328 EYFP group,  $102.8\% \pm 2.2\%$  vs.  $106.7\% \pm 4.8\%$ ,  $P > 0.05$ , [Figure 6h-i](#)) These results suggest  
329 that high frequency activation of  $EC^{CCK+} \rightarrow LA$  switches the AEP-LTP in the LA.

330 In the next experiment, we examined the possibility of other neuroactive molecules that are co-  
331 released with CCK and contribute to HFLS-induced AEP-LTP. We adopted an RNA  
332 interference technique that specifically knockdown the CCK expression in the EC. We  
333 accomplished this by injecting a Cre-dependent AAV cassette carrying a ChR2 variant  
334 (E123T/T159C) and a short hairpin RNA (shRNA) targeting CCK (anti-CCK) or a nonsense  
335 sequence (anti-Scramble) into the EC of CCK-Cre mice ([Figure 7a-c](#)). The inclusion of laser-  
336 responsive ChR2 allowed us to induce the above AEP-LTP by specifically stimulating the  
337  $EC^{CCK+} \rightarrow LA$  pathway. We applied our HFLS pairing protocol in these mice and found that  
338 AEP-LTP could not be induced in the anti-CCK group but could successfully induced in the  
339 anti-Scramble group ([Figure 7d-f](#), two-way RM ANOVA, significant interaction,  $F [1,31] =$   
340  $14.94$ ,  $P < 0.001$ ; pairwise comparison, before vs. after pairing in the anti-CCK group,  $101.5\%$   
341  $\pm 2.5\%$  vs.  $98.0\% \pm 4.8\%$ ,  $P > 0.05$ ; before vs. after pairing in the anti-Scramble group,  $103.0\%$   
342  $\pm 3.8\%$  vs.  $138.8\% \pm 9.7\%$ ,  $P < 0.001$ ). This observation implies that CCK alone is responsible  
343 for HFLS-induced AEP-LTP.

344 To dissect the real-time behavioral dependency of trace fear memory formation on the  
345  $EC^{CCK+} \rightarrow LA$  pathway, we employed optogenetics. We expressed the inhibitory opsin  
346 eNpHR3.0 (AAV-EF1 $\alpha$ -DIO-eNpHR3.0-mCherry) or GFP control (AAV-hSyn-FLEX-GFP)  
347 in the EC of CCK-Cre mice. We also implanted optic fibers targeting the LA in these mice and  
348 then subjected the mice to trace fear conditioning ([Figure 8a-b](#)). During trace fear conditioning,  
349  $EC^{CCK+} \rightarrow LA$  were stimulated at a frequency of 5 Hz (i.e., 100 ms illumination + 100 ms  
350 interval) by the optic fibers for the duration of the CS and trace interval, as indicated in [Figure](#)  
351 [8a](#). For these experiments, mice were positioned in a head-fixed setup on a moveable surface,



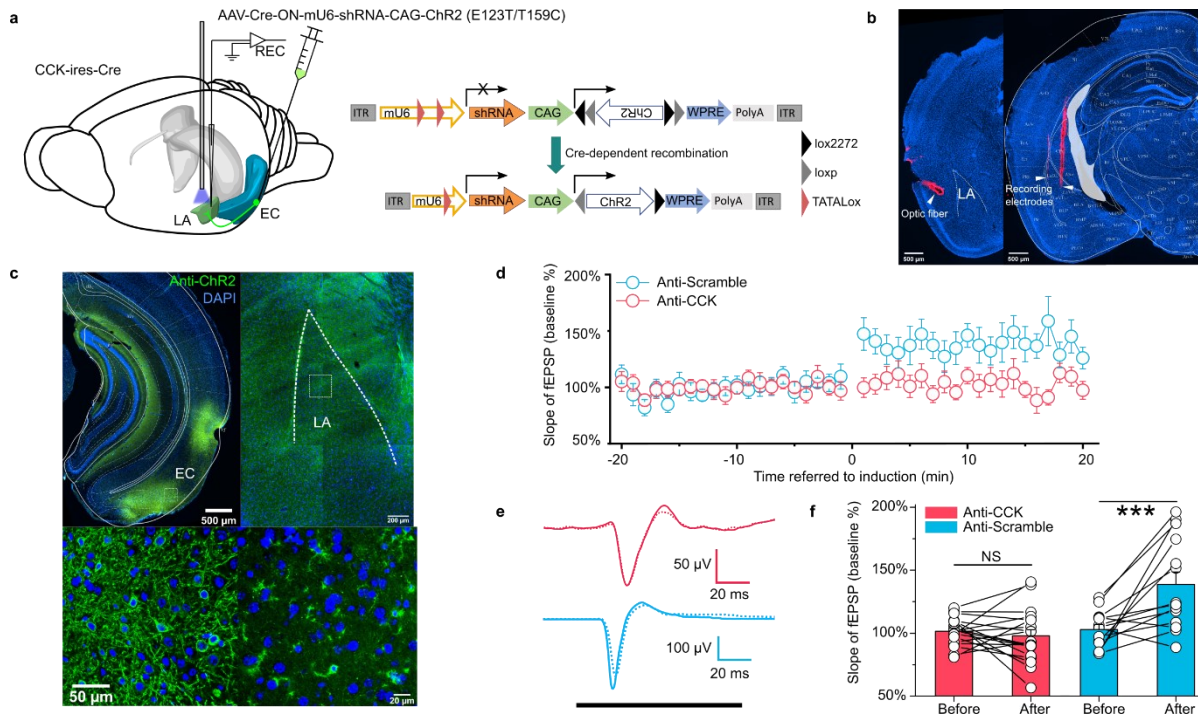


**Figure 7. *In vivo* knockdown of CCK expression blocks AEP-LTP induction in the LA.**

(a) Schematic diagram of the experiment. CCK-Cre mice were injected in the EC with an AAV expressing shRNA (anti-CCK or anti-Scramble) and Chr2. *In vivo* recording was conducted in the LA (left). After Cre-mediated recombination, EC-CCK neurons were transfected with shRNA targeting CCK (anti-CCK) or nonsense sequence (anti-Scramble) as well as the excitatory opsin Chr2 variant E123T/T159C (right). AAV, adeno-associated virus; EC, entorhinal cortex; LA, lateral amygdala; REC, recording; ITR, inverted terminal repeat; mU6, mouse U6 promoter; CAG, CMV enhancer, chicken  $\beta$ -actin promoter; WPRE, woodchuck hepatitis virus (WHP) posttranscriptional regulatory element.

(b) Post-hoc verification of the electrode tracks and optic fiber.

(c) Post-hoc immunofluorescent staining targeting Chr2 in the EC (left) as well as in the CCK-positive projections distributed in the LA (right). Magnified images are shown in the bottom insets.

(d) Time course plot of the normalized AEP slope before and after pairing in mice expressing anti-CCK or anti-Scramble shRNA.

(e) Representative traces of the averaged AEP before (–10–0 min, dotted line) and after (10–20 min, solid line) induction in the two groups. Anti-Scramble is indicated in blue, and anti-CCK is indicated in red.

(f) The average normalized slopes 10 min before pairing (–10–0 min, before) and 10 min after pairing (10–20 min, after) in the two groups. \*\*\* $P < 0.001$ , two-way RM ANOVA with Bonferroni post-hoc pairwise test; RM ANOVA, repeated measures analysis of variance; NS, not significant; fEPSP, field excitatory postsynaptic potential.

352 and an electrical tail shock was given as the US. After administration of the US, we most  
 353 commonly observed flight (running). Interestingly, we found that after a few training trials,  
 354 some GFP control mice (3/6 animals, data not shown) began running before the US was given,

355 suggesting that GFP mice associate the CS with the US and make predictions in subsequent  
356 training trials ([Movie S11](#)). In contrast, we observe much fewer conditioned defensive  
357 responses in the eNpHR group throughout the training process (1/8 animals and 2/40 observed  
358 training trials, data not shown, [Movie S12](#)). Additionally, we recorded the freezing percentages  
359 in response to the CS before and after head-fixed fear conditioning ([Figure 8c–d](#)). We found  
360 that mice in the eNpHR group showed impaired freezing percentages post-training compared  
361 to mice in the GFP group ([Figure 8d](#), two-way RM ANOVA, significant interaction,  $F [1,12]$   
362  $= 19.20$ ,  $P < 0.001$ ; pairwise comparison, GFP vs. eNpHR post-training,  $39.0\% \pm 2.0\%$  vs.  
363  $12.2\% \pm 4.8\%$ ,  $P < 0.001$ ; [Movie S13, S14](#)). We did not observe any differences between the  
364 two groups at baseline ([Figure 8d](#), pairwise comparison, GFP vs. eNpHR at baseline,  $12.7\% \pm$   
365  $3.4\%$  vs.  $12.2\% \pm 4.8\%$ ,  $P > 0.05$ ) or prior to the CS ([Figure 8c](#), two-way RM ANOVA,  
366 interaction not significant,  $F [1, 12] = 0.67$ ,  $P = 0.43$ ; pairwise comparison, GFP vs. eNpHR at  
367 baseline,  $15.0\% \pm 2.8\%$  vs.  $8.0\% \pm 1.7\%$ ,  $P > 0.05$ ; GFP vs. eNpHR post-training,  $19.3\% \pm$   
368  $3.8\%$  vs.  $17.8\% \pm 5.4\%$ ,  $P > 0.05$ ). Altogether, our results suggest that trace fear memory  
369 formation is disturbed by real-time inhibition of the  $EC^{CCK^+} \rightarrow LA$  pathway.

370 In summary, the release of the neuropeptide CCK from the EC neurons switches neural  
371 plasticity in the LA, and facilitates the formation of trace fear memory. Dysfunction in any part  
372 of this pathway impairs the formation of trace fear memory in mice. These results extend our  
373 understanding of learning and memory formation and have important implications for fear-  
374 related mental disorders.

## 375 Discussion

376 Here, we employed classical Pavlovian trace fear conditioning to test the formation of trace  
377 fear memory in  $CCK^{-/-}$  and WT mice. We demonstrate that  $CCK^{-/-}$  mice have impaired fear  
378 responses compared to WT mice in both short and long trace fear conditioning. We also  
379 confirm that this behavioral defect is not caused by other abnormalities, including deficits in  
380 hearing and fear expression. Indeed, we demonstrate that depletion of CCK expression in mice  
381 impairs trace fear conditioning responses, which can be rescued by exogenous activation of  
382 CCKBR with its agonist CCK-4. Overall, our study suggests that trace fear memory formation  
383 and neural plasticity in the LA are dependent on a functional CCK network in the CNS.

384 Trace fear conditioning includes a gap between the CS and the US, which distinguishes it from  
385 the simultaneous CS-US termination in delay fear conditioning. In trace fear conditioning, mice  
386 must retain information from the CS during the trace interval and associate it with the  
387 subsequent US. As a result, the learning process in trace fear conditioning is slower than in  
388 delay fear conditioning, and fear generalization is more pronounced. We previously reported  
389 that WT animals form CS-US associations after three trials with minimal fear generalization in  
390 auditory-cued delay fear conditioning (X. Chen et al., 2019). In our previous report, we also  
391 demonstrated that  $CCK^{-/-}$  mice have difficulties in forming auditory-cued delay fear memory,  
392 visually-cued delay fear memory, or electrically-cued trace fear memory in which an electrical  
393 pulse stimulus in the auditory cortex is paired with a foot shock (X. Chen et al., 2019; Z. Zhang  
394 et al., 2020). Together, the results of our previous work and the present study indicate that the  
395 absence of the neuropeptide CCK has broad damaging effects on multiple forms of fear  
396 memory and is not limited to trace fear memory.

397 Fear conditioning can potentiate the signals of auditory responsive units in the LA (Quirk et  
398 al., 1995) in a phenomenon referred to as LTP. As a result, many studies have identified LTP

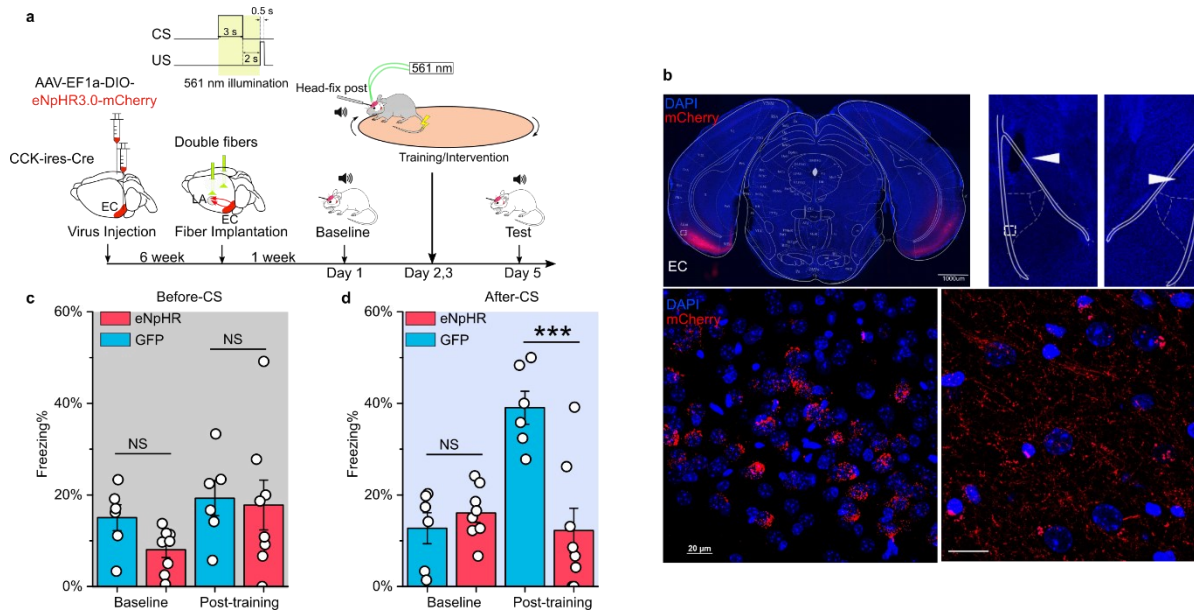


**Figure 8. Real-time inhibition of the EC<sup>CCK+</sup> → LA pathway impairs trace fear memory formation.**

(a) Schematic diagram of the experiment. The Cre-dependent inhibitory opsin eNpHR3.0 was expressed in the EC of CCK-Cre mice. Optic fibers were implanted near the LA to illuminate the CCK-positive fiber that signals from the EC to the LA during auditory-cued trace fear conditioning. The inset at the top right shows the timing of illumination, which covers the CS presentation and trace interval. EC, entorhinal cortex; LA, lateral amygdala; CS, conditioned stimulus; US, unconditioned stimulus.

(b) Post-hoc verification of viral expression in the EC (top left) and of the optic fiber track in the LA (top right). The white rectangle in the top right panel is magnified in the bottom right panel. Magnified images show the transfected EC-CCK neurons (bottom left) and the CCK-positive EC-LA fibers (bottom right).

(c–d) Freezing percentages before (c) and after (d) the CS in eNpHR-expressing mice (red, N = 8) and GFP-expressing control mice (blue, N = 6) on pre-training day (baseline) and post-training day. \*\*\**P* < 0.001; NS, not significant; two-way RM ANOVA with Bonferroni post-hoc pairwise test; RM ANOVA, repeated measures analysis of variance.

399 as a physiological hallmark of fear conditioning (Blair HT, Schafe GE, Bauer EP, Rodrigues  
 400 SM, 2001; Maren, 2001). In our study, we used *in vivo* recording to measure auditory-evoked  
 401 field excitatory postsynaptic potential (fEPSP) or AEP. We did not find any apparent  
 402 abnormalities in AEP (such as amplitude or latency) in CCK<sup>-/-</sup> mice, suggesting that cortical  
 403 and thalamic auditory inputs to the LA were functional. CCK<sup>-/-</sup> mice did fail to induce AEP-  
 404 LTP in the LA, strongly suggesting a deficiency in neural plasticity. However, we cannot  
 405 simply assume that AEP-LTP induction is equivalent to trace fear memory. Occasionally, AEP-  
 406 LTP is not sufficient to trigger the expression of fear behaviors. Kim and Cho reported that  
 407 LTP in the LA was maintained during fear extinction (Kim & Cho, 2017). Thus, LTP in the  
 408 LA is necessary but not sufficient for fear memory formation.

409 As the EC has been previously implicated in trace fear memory and behaviors, we manipulated  
 410 EC function in our present study and investigated the behavioral and signaling outcomes. We  
 411 found that silencing EC neurons with DREADD hm4Di impaired the formation of trace fear  
 412 memory, which is consistent with several previous studies. For instance, electrolytic lesion of

413 the EC impairs trace eyeblink conditioning performance in mice (Ryou et al., 2001), and  
414 neurotoxic lesions as well as M1 receptor blockade in the EC impair trace fear memory  
415 formation but not delay fear memory formation (Esclassan et al., 2009). Although this  
416 preferential association with trace fear memory has also been observed in certain areas of the  
417 hippocampus (Bangasser, 2006), the EC is a promising regulatory unit, because EC neurons  
418 maintain persistent spikes activity in response to stimuli (Egorov et al., 2002; Fransén et al.,  
419 2006). This sustained neuronal activity is thought to be the neural basis of ‘holding’ CS  
420 information during trace intervals to allow for CS-US association even after long trace intervals  
421 (20 seconds in our study). This information ‘holding’ theory is consistent with neuroimaging  
422 reports on working memory in subjects who ‘hold’ stimuli for specific periods (Nauer et al.,  
423 2015).

424 Auditory responses have been previously found in the EC and its upstream circuit (G. W. Zhang  
425 et al., 2018), however, these responses were limited to loud noise and did not involve the pure  
426 tone used in our behavioral paradigm. We reasoned that if the EC perceives and delivers the  
427 CS to downstream structures, then lesions in the EC would disturb the delay fear conditioning  
428 as well. Instead, previous studies have robustly demonstrated that EC lesions leave delay fear  
429 memory intact (Esclassan et al., 2009). The amygdala responds directly to the AS, and receives  
430 inputs from the AC, the MGB, and hippocampus directly. Thus, the EC is likely involved in  
431 the CS-US association in a more complicated manner, and this mechanism requires further  
432 investigation. We speculate that this mechanism is probably similarly as our previous finding  
433 in the sound-sound association (X. Chen et al., 2019) and visuo-auditory association (Z. Zhang  
434 et al., 2020), which is neuropeptide-based hetero-synaptic modulation machinery.

435 With cell type-specific tracing systems, we demonstrated that the EC is an upstream brain  
436 region that projects CCK-positive afferents to the LA, and these CCK-expressing EC neurons  
437 are primarily excitatory (Figure 3). Using anterograde Cre-dependent color switch labeling in  
438 the EC, we also found that CCK-expressing neurons were the predominant source of EC-LA  
439 projections, implying that CCK is integral to EC-LA connection and communication. Cell type-  
440 specific chemogenetic inhibition of CCK-expressing neurons in the EC also impaired the  
441 formation of trace fear memory. However, we cannot exclude the possibility that CCK may  
442 originate in other brain regions and contribute to fear memory formation.

443 We triggered the release of CCK from axon terminals after *in vivo* HFLS of CCK-expressing  
444 fibers in the LA (Hököfelt, 1991). In the presence of this artificially released CCK neuropeptide,  
445 we then presented the AS. The AS activates presynaptic axons via the canonical LA fear circuit,  
446 which is supported by the known role of the LA in receiving auditory input from both the  
447 auditory cortex and the thalamus (Romanski & LeDoux, 1992). In our study, the AS triggered  
448 postsynaptic neural firing. Therefore, our HFLS-mediated AEP-LTP induction protocol  
449 combines the released CCK with pre- and postsynaptic activation altogether in the LA and this  
450 pairing leads to the potentiation of AEP in the LA.

451 In the current study, we successfully excluded the contribution of substances co-released with  
452 CCK to the induction of AEP-LTP by applying the *in vivo* RNA interference to knockdown  
453 the expression of *Cck* in CCK-positive neurons of the EC. We found that knockdown of *Cck*  
454 blocked the induction of AEP-LTP and our *in vivo* application of shRNA supports the clinical  
455 use of shRNA to target mental disorders related to the CCK system. Our results that the  
456 inhibition of CCK-positive EC afferents to the LA impaired trace fear memory formation  
457 during both the learning and response phases suggest that establishing the CS-US association  
458 during trace fear conditioning requires functional CCK-positive EC-LA projections.

459 In conclusion, we found that EC-LA projections modulate neuroplasticity in the LA and  
460 therefore contribute to the formation of trace fear memory. The CCK terminals of the EC  
461 neurons in the LA release CCK that enable hetero-synaptic neuroplasticity of the auditory  
462 pathway to the LA. Our findings add a novel insight into the participation of the neuropeptide  
463 CCK in the formation of the trace fear memory. As various mental disorders, including anxiety  
464 (Davis, 1992), depression (Shen et al., 2019; Siegle et al., 2007), and PTSD (Shin et al., 2006),  
465 are highly correlated with hyperactivation and dysfunction of the amygdala and the fear  
466 memory circuitry, our finding supports CCK and its receptors as potential new targets for future  
467 therapeutic applications in these disorders.

468

## 469 **Acknowledgments**

470 **Funding:** The authors thank Eduardo Lau for administrative and technical assistance. This  
471 work was supported by Hong Kong Research Grants Council (T13-605/18-W, 11102417M,  
472 11101818M, 11103220), Natural Science Foundation of China (31671102), Health and  
473 Medical Research Fund (06172456 and 31571096), Innovation and Technology Fund  
474 (MRP/101/17X, MPF/053/18X, GHP\_075\_19GD). We also thank the following charitable  
475 foundations for their generous supports to JH: Wong Chun Hong Endowed Chair Professorship,  
476 Charlie Lee Charitable Foundation, and Fong Shu Fook Tong Foundation.

## 477 **Author Contributions**

478 JH, HF and XC designed the experiments; HF conducted the electrophysiological and  
479 behavioral experiments in mice; JS designed and manufactured two AAVs; HF, WF collected  
480 the data of behavioral experiments; HF, WF collected and analyzed the anatomy data; JH, and  
481 HF wrote the manuscript.

## 482 **Declaration of Interests**

483 The authors declare no conflict of interest.

## 484 **Materials and Methods**

485 **Table 1. Key Resources**

REAGENT or RESOURCE	SOURCE	IDENTIFIER
<b>Antibodies</b>		
Anti-CCKBR (1:1000)	Thermo Fisher Scientific, Waltham, MA, USA	Cat# PA3-201, RRID: AB_10979062
Anti-CCKBR (1:200)	Santa Cruz Biotechnology, Dallas, TX, USA	Cat# sc-166690, RRID: AB_2070487
Anti-Synaptophysin (1:500)	Sigma-Aldrich, St. Louis, MO, USA	Cat# S5768, RRID: AB_477523
Anti-CamKII $\alpha$ (1:500)	Abcam, Cambridge, UK	Cat# Ab52476, RRID: AB_868641
Anti-GAD67 (1:500)	Millipore, Burlington, MA, USA	Cat# MAB5406, RRID: AB_2278725
Anti-ChR2 (1:2000)	American Research Products, Waltham, MA, USA	Cat# 03-651180
Alexa647 Donkey-anti-Mouse (1:500)	Jackson ImmunoResearch Labs, West Grove, PA, USA	Cat# 715-605-150, RRID: AB_2340862
Alexa647 Donkey-anti-Rabbit (1:500)	Jackson ImmunoResearch Labs, West Grove, PA, USA	Cat# 711-605-152, RRID: AB_2492288
DyLight 594 Goat-anti-Mouse (1:500)	Thermo Fisher Scientific, Waltham, MA, USA	Cat# 35511, RRID: AB_1965950
Alexa488 Donkey-anti-Mouse (1:500)	Jackson ImmunoResearch Labs, West Grove, PA, USA	Cat# 715-545-150, RRID: AB_2340846
Alexa594 Goat-anti-Mouse (1:500)	Jackson ImmunoResearch Labs, West Grove, PA, USA	Cat# 111-585-144, RRID: AB_2307325
<b>Virus</b>		
AAV-Ef1 $\alpha$ -DIO-ChETA-EYFP	Addgene, Watertown, MA, USA	RRID: Addgene_26968
AAV-EF1 $\alpha$ -DIO-EYFP	BrainVTA, Wuhan, China	NA
AAV-hSyn-FLEX-GFP	BrainVTA, Wuhan, China	NA
AAV-hSyn-hM4Di-EGFP	BrainVTA, Wuhan, China	NA
AAV-hSyn-EGFP	Addgene, Watertown, MA, USA	RRID: Addgene_105539
AAV-hSyn-DIO-hM4D(Gi)-mCherry	Addgene, Watertown, MA, USA	RRID: Addgene_44362
AAV-hSyn-DIO-mCherry	Addgene, Watertown, MA, USA	RRID: Addgene_50459
AAV-EF1 $\alpha$ -DIO-eNpHR3.0-mCherry	BrainVTA, Wuhan, China	NA
AAV-EF1 $\alpha$ -FAS-EGFP	Taitool, Shanghai, China	NA

AAV-CAG-DO-mCherry-DIO-EGFP	This paper	NA
AAV8-Cre-ON-ChR2-antiCCK	This paper	NA
AAV8-Cre-ON-ChR2-antiScramble	This paper	NA
retroAAV-hSyn-FLEX-jGcamp7s	Addgene, Watertown, MA, USA	RRID: Addgene_104491
AAV-hSyn-CCK2.0	Vigene Bioscience, Ji'nan, China	NA
<b>Oligonucleotides</b>		
Anti-CCK	BGI, Shenzhen, China	GACTCCCAGACCTAATG TTGC
Anti-Scramble	BGI, Shenzhen, China	GTTGGCTCCTAGCAGAT CCTA
Primers for genotyping of CCK <sup>-/-</sup>	BGI, Shenzhen, China	ATGCAGGCAAATTTTGG TGT; GAGCGGACACCCTTACC TTT; GACTTCTGTGTGCGGGA CTT
<b>Recombinant DNA</b>		
pAAV-CAG-Flex-tdTomato	Addgene	28306
PUC57-mU6 with TATALox		
PUC57-CAG-DIO-ChR2(E123T/T159C)-Flag	Addgene	35509; 101766
pUC57-CAG-DIO-mCherry-EYFP (inverted)	Addgene	34582; 98750
<b>Chemicals, Peptides, and Recombinant Proteins</b>		
Urethane	Sigma-Aldrich, St. Louis, MO, USA	Cat# U2500
Pentobarbital (20% Dorminal)	Alfasan International B.V., Woerden, Netherlands	
CCK4	Abcam, Cambridge, UK	Cat# ab141328
Dil Stain	Thermo Fisher Scientific, Waltham, MA, USA	Cat# D282
Clozapine	Sigma-Aldrich, St. Louis, MO, USA	Cat# C6305
Alexa Fluor 647-conjugated Cholera Toxin Subunit B	Thermo Fisher Scientific, Waltham, MA, USA	Cat# C34778
<b>Experimental Models: Organisms/Strains</b>		
Mouse: C57BL/6	The Laboratory Animal Services Centre, Chinese University of Hong Kong, Laboratory Animal Research Unit, City University of Hong Kong	
Mouse: CCK-ires-Cre	The Jackson Laboratory, Bar Harbor, ME, USA	Cck <sup>tm1.1(Cre)Zjh/J</sup> , Stock No: 012706



Mouse: CCK-CreER	The Jackson Laboratory, Bar Harbor, ME, USA	Cck <sup>tm2.1(tm2.1/ERT2)Zjh/J</sup> , Stock No: 012710
Mouse: CCK-ABKO	The Jackson Laboratory, Bar Harbor, ME, USA	Stock No: 006365
Mouse: CCK-BR KO	The Jackson Laboratory, Bar Harbor, ME, USA	Stock No: 006369
<b>Software and Algorithms</b>		
Origin 2018	OriginLab, Northampton, MA, USA	
Matlab R2020a	Mathworks, Natick, MA, USA	
Fiji	(Schindelin et al., 2012)	<a href="https://imagej.net/Fiji">https://imagej.net/Fiji</a>
TDT OpenEX	Tucker-Davis Technologies, Alachua, FL, USA	
Photoshop CC	Adobe, San Jose, CA, USA	
Excel	Microsoft, Redmond, WA, USA	
Inkscape		<a href="https://inkscape.org/">https://inkscape.org/</a>
Offline Sorter	Plexon, Dallas, TX, USA	
NeuroExplorer	Plexon, Dallas, TX, USA	
Bonsai	(Lopes et al., 2015)	<a href="https://bonsai-rx.org/">https://bonsai-rx.org/</a>
CellProfiler	(McQuin et al., 2018)	<a href="https://cellprofiler.org/">https://cellprofiler.org/</a>

486

## 487 **Animals**

488 Adult male and female C57BL/6, CCK<sup>-/-</sup> (CCK-CreER), and CCK-Cre (CCK-ires-Cre) mice  
489 were used in experiments. For behavioral experiments, only adult male mice were used. Mice  
490 were housed in a 12 hour light/12 hour dark cycle (dark from 08:00 to 20:00) and were provided  
491 food and water *ad libitum*. All experimental procedures were approved by the Animal Subjects  
492 Ethics Sub-Committee of the City University of Hong Kong.

493 For surgical procedures when doing virus injection and optic fiber implantation, mice were  
494 anesthetized with pentobarbital sodium (80 mg/kg, i.p., 20% Dorminal, Alfasan International  
495 B.V., Woerden, Netherlands,). For acute electrophysiological recording, mice were  
496 anesthetized with pentobarbital sodium (80 mg/kg, i.p.) or urethane sodium (2 g/kg, i.p.,  
497 Sigma-Aldrich, St. Louis, MO, USA). Both anesthetics were periodically supplemented during  
498 the experiment to maintain anesthesia. Mice were fixed in a stereotaxic device, and the scalp  
499 was incised. A local anesthetic (xylocaine, 2%) was applied to the incision site for analgesia.  
500 After skull levelling, craniotomies were performed with varying parameters based on the region  
501 of the brain being accessed.

## 502 **Auditory and visual stimuli**

503 Auditory stimuli, including pure tones and white noise, were digitally generated by a  
504 specialized auditory processor (RZ6 from Tucker-Davis Technologies [TDT], Alachua, FL,  
505 USA). For behavioral experiments, auditory stimuli were delivered via a free-field magnetic  
506 speaker (MF-1, TDT) mounted 60cm above the animal. Sound intensity was adjusted by a  
507 condenser microphone (Center Technology, Taipei) to ~70 dB when it reached the animal. For  
508 *in vivo* recording, auditory stimuli were delivered via a close-field speaker placed

509 contralaterally to the recording side. The sound intensity that induced 50%–70% of the  
510 maximum response was selected. Visual stimuli were generated by a direct current (DC)-driven  
511 torch bulb via the analog voltage output of the TDT workstation. Light intensity was roughly  
512 quantified as the value of the trigger voltage. For *in vivo* recording, the light intensity that  
513 induced 50%–70% of the maximum response was selected.

#### 514 **Auditory brainstem response recording**

515 Mice were anesthetized with pentobarbital sodium (80 mg/kg, i.p.) and placed on a clean and  
516 warm blanket in a soundproof chamber. A free-field magnetic speaker (MF-1, TDT) was placed  
517 10 cm away from the right ear of mice. Recording, reference and ground needle electrodes  
518 (Spes Medica, Genova, Italy) were subcutaneously inserted below the forehead, right ear and  
519 left ear, respectively. Auditory stimuli (wide spectrum clicks, 0.1 ms) were presented to the  
520 mouse with a decreasing level from 80 dB to 20 dB with an interval of 5 dB. For each level of  
521 click stimulus, total 512 times of presentation were given at a frequency of 21 Hz. ABR signals  
522 were collected via a specialized processor (RZ6, TDT) and digitalized with a bandpass filter  
523 from 100 Hz to 5 kHz. Stimuli generation and data processing was performed with software  
524 BioSigRZ (TDT).

#### 525 **Trace fear conditioning**

526 On pre-conditioning day, each mouse was placed into the testing context (acrylic box with  
527 white wallpaper measuring 25 cm × 25 cm × 25 cm) for habituation and baseline recording.  
528 After 3 min of habituation, a CS (2.7 kHz or 8.2 kHz pure tone, 70 dB SPL, 3 s for the short  
529 trace paradigm and 10 s for the long trace paradigm) was given three times within 20 min.

530 On conditioning day, the mouse was placed into the fear conditioning context (acrylic box with  
531 brown wallpaper measuring 18 cm wide × 18 cm long × 30 cm high and equipped with foot  
532 shock stainless steel grid floor). After 3 min of habituation, a CS-US pairing was given. In the  
533 short trace interval paradigm, an US (0.5 mA foot shock, 0.5 s) was given 2 s after a 3-s-long  
534 CS. Three trials were given on each training day, and the interval between trials was 10–15  
535 min. Totally two training days were given. The mouse was kept in the fear conditioning context  
536 for a 10 min consolidation period after the last training trial. In the long trace interval paradigm,  
537 an US was given 20 s after a 10-s-long CS. Eight training trials were given each training day,  
538 and the interval between trials was 2–3 min. The mouse was kept in the fear conditioning  
539 context for a 5 min consolidation period after the last training trial. After training, each animal  
540 was kept in a temporary cage and returned to their home cage after all individuals finished  
541 training.

542 On post-conditioning day (test day), the mouse was placed into the testing context. After 3 min  
543 of habituation, a CS was presented to the animal twice with a 2 min-long interval between  
544 stimuli. Two min after the last trial, the animal was transferred to a temporary cage and returned  
545 to its home cage after all individuals in its cage finished testing.

546 All contexts were cleaned thoroughly with 75% ethanol after each individual session. All of  
547 the above procedures were conducted in a soundproof chamber, and all videos (baseline,  
548 training, and testing) were recorded with a webcam (Logitech C270) set in the ceiling of the  
549 chamber. Videos were analyzed with a custom program based on an open-source platform  
550 (Lopes et al., 2015) (<https://bonsai-rx.org>). Briefly, the centroid of the animal was extracted  
551 from the videos. By comparing the coordinates of the centroid frame by frame, we then  
552 calculated the distance moved between two frames. The instant velocity of the animal was  
553 calculated by dividing this distance by the time span between two adjacent frames. The freezing  
554 percentage was defined as the percentage of frames with an instant velocity lower than the  
555 threshold of all frames in an observed time window. We compared the output of this program

556 to results observed by the naked eye. Finally, we selected 0.1 (pixel<sup>2</sup>/s) as the appropriate  
557 moving threshold to define freezing. Freezing score was defined as the binary value (0 or 1) of  
558 time frame with instant velocity higher (0, ‘not freezing’) or lower (1, ‘freezing’) than the  
559 threshold. For freezing score plot shown in Figure 1, 2 and 4, freezing scores from all test  
560 sessions were averaged per second for data visualization.

### 561 **Electrophysiological recording in the LA and EC**

562 Mice were subjected to the surgical procedures describe above. Tracheotomy was conducted  
563 to facilitate breathing and to prevent asphyxia caused by tracheal secretions during the  
564 experiment. Craniotomy was performed 1.0–2.0 mm posterior and 3.0–4.0 mm lateral to the  
565 bregma to target the LA. Dura mater was partially opened using a metal hook made of a 29G  
566 syringe needle. Tungsten recording electrodes (0.5–3.0 MΩ, FHC, Bowdoin, ME USA) were  
567 slowly inserted into the LA (approximately 3.5 mm from the brain surface). For laser  
568 stimulation experiments, another craniotomy was performed at the temporal lobe (1.0-2.0 mm  
569 posterior to the bregma) to expose the lateral rhinal vein. One optic fiber (200 μm diameter,  
570 0.22 NA, Thorlabs, Newton, NJ, USA) was inserted below the rhinal vein and forwarded till  
571 1.0–1.5 mm from the surface. The angle of the optic fiber was approximately 75° from the  
572 vertical reference. Responses were recorded and passed to a pre-amplifier (PZ5, TDT) and an  
573 acquisition system (RZ5D, TDT). Signals were filtered for field potential or spikes with  
574 respective bandwidth ranges of 10–500 Hz and 1–5000 Hz. All recordings were stored using  
575 TDT software (OpenEx, TDT). The maximum sound intensity was defined as the intensity that  
576 elicited a saturated AEP. The AEP baseline was recorded with 50% of the maximum sound  
577 intensity at a 5 s intertrial interval (ITI) for 20 min. For high-frequency electrical stimulation  
578 (HFS) experiments, we used ~ 70% of the maximum sound intensity and a 150 μA electrical  
579 stimulation current. For high-frequency laser stimulation (HFLS) experiments, we used > 10  
580 mW laser power to ensure activation of transfected axons. After AEP-LTP induction, we  
581 recorded the AEP for another 20 min.

582 For recording in the EC, we applied the protocol from the Li I. Zhang laboratory (G. W. Zhang  
583 et al., 2018). Craniotomy was performed at the juncture of the temporal, occipital, and  
584 interparietal bones and exposed the caudal rhinal vein and the transverse sinus ([Figure S3](#)).  
585 Electrodes were inserted approximately 1 mm below the dura mater.

586 All field potential data were extracted and processed in the MATLAB program, and all single  
587 unit data were extracted from the TDT data tank to the Offline Sorter (Plexon) for spike sorting.  
588 Sorted data were forwarded to the Neuroexplorer (Plexon) for additional processing and  
589 visualization.

### 590 **Plasmid construction and AAV packaging**

591 The sequence and cloning details of plasmid will be described elsewhere (Su et al., manuscript  
592 in preparation). In principle, we generated AAV vectors that allow Cre-controlled expression  
593 of shRNA and channelrhodopsin in neurons. For plasmid pAAV-Cre-ON-mU6-ShRNA-CAG-  
594 ChR2(E123T/T159C), shRNA was placed under the control of a mouse U6 (mU6) promoter  
595 inserted with a TATALox element (Ventura et al., 2004). CAG-DIO-ChR2(E123T/T159C)  
596 cassette was inserted following the mU6-TATALox-ShRNA cassette.

597 In brief, the pAAV backbone was recovered after digesting pAAV-CAG-Flex-tdTomato  
598 (Addgene 28306) with NdeI and HindIII. Fragment 1 (pUC57-Cre-ON-mU6-shRNA) was  
599 acquired by digesting pUC57-Cre-ON-mU6(TATALox) with HpaI and XhoI and then ligating  
600 it with annealed oligos that targets the coding sequence of Cck mRNA (Anti-CCK) or nonsense  
601 sequence (Anti-Scramble). Fragment 2 was acquired by digesting pUC57-CAG-DIO-  
602 ChR2(E123T/T159C)-Flag) with XhoI and HindIII. Fragment 3 was acquired by digesting

603 pUC57-CAG-DIO-mCherry-EYFP (inverted)) with EcoRI and HindIII. pAAV backbone,  
604 Fragment 1 and Fragment 2 was ligated to make pAAV-Cre-ON-mU6-ShRNA-CAG-DIO-  
605 ChR2 (E123T/T159C)-Flag. pAAV backbone, Fragment 1 without shRNA, Fragment 3 was  
606 ligated to make pAAV-CAG-DO-mCherry-DIO-EYFP. DNA templates and shRNA oligoes  
607 mentioned above were acquired from Addgene or synthesized from BGI (Shenzhen, China)  
608 and verified by sequencing.

609 For AAV packaging (Xiong et al., 2015), HEK293T cells were seeded into 5 dishes (15cm,  
610 poly-D-lysine coated) for 1 viral preparation one day before transfection. Standard medium  
611 (DMEM, +10% FBS and antibiotics) were used for HEK293T cells. For PEI transfection, mix  
612 35 µg AAV8 helper plasmid, 35 µg AAV vector, 100 µg pHGTI-adenol, 510 µL of PEI (1  
613 µg/mL, Sigma) with DMEM (without FBS or antibiotics) to final volume of 25 mL. Incubate  
614 this mixture at room temperature for 15 min. Meanwhile, replace the media in dishes with  
615 DMEM + 10% NuSerum (Bio-gene) + antibiotics (20 mL/plate). Then add 5 mL of  
616 transformation mix per plate. 24 hours after transfection, change the culture media to DMEM  
617 + antibiotics without Serum. 72 hours after transfection, culture medium was collected and  
618 filtered to get rid of cell pellets. Collected medium was stirred at 4 °C for 1.5 hours, meanwhile  
619 mixed with NaCl (final concentration of 0.4 M) and PEG8000 (final concentration of 8.5%  
620 w/v). Virus were precipitated by centrifugation at 7000 g for 10 min. Supernatant was discarded  
621 and 10 mL lysis buffer (150 mM NaCl, 20 mM Tris pH = 8.0) was added to re-suspend the  
622 virus pellet. Virus was then concentrated and purified via Iodixanol gradients (“Optiprep”  
623 Sigma D1556-250mL). Centrifuge the gradients for 90 min at 46,500 rpm at 16 °C. The virus  
624 in 40% fraction was harvested and mixed with PBS and then transferred to an Amacon 100K  
625 columns- UFC910008 to remove the Iodixanol. Purity and titer of virus were then assessed by  
626 SDS-PAGE and SYPRO ruby staining (S-12000, Life technologies, Carlsbad, CA, USA ).

### 627 **Viral and tracer injection**

628 Mice were subjected to the surgical procedures described above. For viral injection into the EC,  
629 the following rostral parameters were used: Anterior-Posterior (AP) = 3.25 mm, Medial-Lateral  
630 (ML) = 3.80 mm, Dorsal-Ventral (DV) = 3.60 mm from the surface, volume = 100 nL.  
631 Similarly, the following caudal parameters were used: AP = 4.25 mm, ML = 3.60 mm, DV =  
632 2.60 mm from surface, volume = 200 nL. For injection of tracer or virus into the LA, we used  
633 the following parameters: AP = 1.70 mm, ML = 3.40 mm, DV = 3.70 mm from the surface,  
634 volume = 200 nL. Craniotomy was performed after skull levelling and partial opening of the  
635 dura mater using a syringe needle hook (29G). We used the Nanoliter2000 system (World  
636 Precision Instruments [WPI], Sarasota County, FL, USA) for all infusions. Viral or tracer  
637 infusions were slowly pumped into brain tissue trough a fine-tip glass pipette filled with silicon  
638 oil at a speed of no more than 50 nL/min. After infusion, the pipette was left in the injection  
639 site for an extra 5–10 min before slow withdrawal. After withdrawal of the pipette, the scalp  
640 was sutured, and a local anesthetic was applied. The animal was returned to its home cage after  
641 awaking. For axon stimulation (observation), the virus was expressed for at least 7 weeks, and  
642 for cell body stimulation (observation), the virus was expressed for at least 4 weeks. For CTB  
643 tracer labeling, we perfused animals after 7 days of viral expression.

### 644 **Optic fiber implantation**

645 Mice were subjected to the surgical procedures described above. Craniotomy was performed  
646 bilaterally to target the LA using the coordinates described above. Optic fibers (optic cannulae)  
647 were gently inserted into the LA (50–100 µm above the target area) and fixed with dental  
648 cement (mega PRESS NV + JET X, megadental GmbH, Bidingen, Germany). For head  
649 fixation, a long screw was fixed to the skull with dental cement at a 45° angle from the vertical  
650 axis.

## 651 **Fiber photometry**

652 The commercial 1-site Fiber Photometry System (Doric Lenses Inc, Quebec, Canada) coupled  
653 with the RZ5D processor (TDT, USA) was used in the current study. Excitation light at 470  
654 nm and 405 nm was emitted from two fiber-coupled LEDs (M470F3 and M405FP1, Thorlabs)  
655 and sinusoidally modulated at 210 Hz and 330 Hz, respectively. The intensity of the excitation  
656 light was controlled by an LED driver (LEDD1B, Thorlabs) connected with the RZ5D  
657 processor via the software Synapse. Excitation light was delivered to the animal through a  
658 dichroic mirror embedded in single fluorescence MiniCube (Doric Lenses, Quebec, QC,  
659 Canada) in a fiber-optic patch cord (200  $\mu$ m, 0.37 NA, Inper, Hangzhou, China). The intensity  
660 of the excitation light at the tip of the patch cord was adjusted to less than 30  $\mu$ W to avoid  
661 photobleaching. The emission fluorescence was collected and transmitted through a bandpass  
662 filtered by the MiniCube. The fluorescent signal was then detected, amplified, and converted  
663 to an analog signal by the photoreceiver (Doric Lenses). Finally, the analog signal was  
664 digitalized by the RZ5D processor and analyzed using Synapse software at 1 kHz with a 5 Hz  
665 low-pass filter.

666 Optical fiber implantation and fiber photometry were used to visualize CCK activity in vivo  
667 via a fluorescent sensor. Briefly, the GPCR-activation-based CCK sensor (GRAB<sub>CCK</sub>, AAV-  
668 hSyn-CCK2.0) was developed by inserting a circular-permuted green fluorescent protein  
669 (cpEGFP) into the intracellular domain of CCKBR (Jing et al., 2019). Binding of CCKBR with  
670 its endogenous or exogenous ligand (CCK) induces a conformational change in cpEGFP and  
671 results in increased fluorescence intensity, which we measured by fiber photometry.

## 672 **Chemogenetic manipulation**

673 Each animal (with DREADD virus injection) received CLZ (0.5 mg/kg, Sigma-Aldrich,  
674 dissolved with 0.1% DMSO) or vehicle (sterilized saline with 0.1% DMSO) by intraperitoneal  
675 injection. After injection, animals were kept in transfer cages for 30 min to allow the drug to  
676 penetrate the blood-brain-barrier (BBB) and bind to the DREADD receptor (Gomez et al.,  
677 2017). Animals were then placed in conditioning boxes for further training.

## 678 **Optogenetic manipulation**

679 CCK-Cre mice were injected with AAV-EF1 $\alpha$ -DIO-eNpHR3.0-mCherry or control AAV-  
680 hSyn-FLEX-GFP. After 7 weeks, animals received bilateral optic fiber implantation as  
681 described above. Mice were allowed a 1-week recovery period to adjust to the head-fix setup.  
682 Baseline freezing percentages were recorded in the testing context on the pre-conditioning day  
683 as described above. On the conditioning day, mice were head-fixed, and limbs were allowed to  
684 move freely on a smooth-rotatory round plate. Optic cables were connected to the implanted  
685 optic cannulae after cleaning the cannulae ends with 75% alcohol. Short trace training  
686 procedures were performed as described above with two exceptions. First, the US was  
687 delivered to the tail by attached wires. Second, the current was increased to 1.0 mA, because  
688 the fur on the tail can hamper perception of electrical shock. A 561 nm green laser (10–20 mW)  
689 was applied from the onset of the CS to the onset of the US with a frequency of 5 Hz (100 ms  
690 illumination + 100 ms interval). On post-conditioning day, the conditioned response of the  
691 animal was recorded in the fear conditioning context. All activity was captured by a camera on  
692 the ceiling and analyzed with the previously-described Bonsai program.

## 693 **Anatomy and immunohistochemistry**

694 Animals were anesthetized with an overdose of pentobarbital sodium, perfused with ice-cold  
695 phosphate buffered saline (PBS, 0.01 M, Sigma-Aldrich), and fixed with paraformaldehyde  
696 solution (PFA, 4% in PBS, Santa Cruz Biotechnology, Dallas, TX, USA). Animals were  
697 decapitated, and the brain was gently removed and submerged into 4% PFA solution for

698 additional fixation (~48 hours). Brains were sectioned into 40- $\mu$ m-thick slices on vibratome  
699 (Leica VT1000 S). To observe viral expression, neural tracer labeling, or electrode track  
700 verification, sections were counter-stained with DAPI (1:10000, Santa Cruz Biotechnology)  
701 for 10 min and mounted onto slides with 70% glycerol (Santa Cruz Biotechnology) in PBS.  
702 For immunohistochemistry, sections were washed with 0.01 M PBS three times for 7 min each  
703 and blocked with blocking solution (5% goat serum and 0.1% triton X-100 in PBS) at room  
704 temperature for 1.5 hours. Each primary antibody was diluted to the appropriate concentration  
705 ([Table 1](#)) in blocking solution and incubated on sections overnight at 4°C. The next day,  
706 sections were washed with PBS three times for 7 min each and stained with secondary antibody,  
707 which was prepared in PBST (0.1% triton X-100 in PBS). Each secondary antibody was  
708 incubated on sections at room temperature for 3 hours. After secondary incubation, the sections  
709 were washed with PBS three times for 7 min each and counter stained with DAPI for 10 min.  
710 Finally, sections were washed three times with PBS and mounted onto slides with 70% glycerol  
711 mounting medium. Fluorescent images were captured with a Nikon Eclipse Ni-E upright  
712 fluorescence microscope and a Zeiss LSM880 confocal microscope.

### 713 **Image analysis**

714 Imaging signal analysis, including quantification of intensity and percent positivity, was  
715 conducted in Fiji(<https://imagej.net/Fiji>) (Schindelin et al., 2012). To quantify the number  
716 (percentage) of viral- or immunohistochemical-positive neurons, we used the Cell Counter  
717 plugin in Fiji. To quantify the projection intensity of viral-positive neural fibers, we used the  
718 FeatureJ plugin in Fiji. We applied Hessian filter to extract the fiber-like structures and  
719 converted the raw images to eigen images with smallest eigen values selected. Eigen images  
720 were then converted to binary image by applying a threshold in Fiji and pixel density was  
721 measured as the intensity of neural projection (Grider et al., 2006). To quantify the  
722 colocalization of the CCK+ terminal (CCK-EYFP and synaptophysin double positive) and the  
723 CCKBR-innervating CCK+ terminal (CCK-EYFP, synaptophysin, and CCKBR triple  
724 positive), we extracted the double positive and triple positive pixels in Fiji and adopted the  
725 pixel-based colocalization analysis algorithm from CellProfiler  
726 (<https://cellprofiler.org/examples>) (McQuin et al., 2018) to calculate the colocalization ratios.

### 727 **Statistical analysis**

728 Group data are shown as mean  $\pm$  SEM (standard error of the mean) unless otherwise stated.  
729 Statistical analyses, including two sample t tests, paired sample t tests, one-way RM ANOVA  
730 (repeated measures analysis of variance), and two-way RM ANOVA, were conducted in Origin  
731 2018 (OriginLab, Northampton, MA, USA). Statistical significance was defined as  $P < 0.05$   
732 by default.

## 733 **References**

- 734 Armbruster, B. N., Li, X., Pausch, M. H., Herlitze, S., & Roth, B. L. (2007). Evolving the lock  
735 to fit the key to create a family of G protein-coupled receptors potently activated by an  
736 inert ligand. *Proceedings of the National Academy of Sciences*, 104(12), 5163–5168.  
737 <https://doi.org/10.1073/pnas.0700293104>
- 738 Bangasser, D. A. (2006). Trace Conditioning and the Hippocampus: The Importance of  
739 Contiguity. *Journal of Neuroscience*, 26(34), 8702–8706.  
740 <https://doi.org/10.1523/jneurosci.1742-06.2006>
- 741 Berna, M. J., Tapia, J. A., Sancho, V., & Jensen, R. T. (2007). Progress in developing

- 742 cholecystokinin (CCK)/gastrin receptor ligands that have therapeutic potential. *Current*  
743 *Opinion in Pharmacology*, 7(6), 583–592. <https://doi.org/10.1016/j.coph.2007.09.011>
- 744 Blair HT, Schafe GE, Bauer EP, Rodrigues SM, L. J. (2001). Synaptic Plasticity in the Lateral  
745 Amygdala: A Cellular Hypothesis of Fear Conditioning. *Learning & Memory*, 8(5), 229–  
746 242. <https://doi.org/10.1101/lm.30901>
- 747 Bradwejn, J. (1993). Neurobiological investigations into the role of cholecystokinin in panic  
748 disorder. *Journal of Psychiatry and Neuroscience*, 18(4), 178–188.
- 749 Chen, Q., Nakajima, A., Meacham, C., & Tang, Y.-P. (2006). Elevated cholecystokinergic  
750 tone constitutes an important molecular/neuronal mechanism for the expression of anxiety  
751 in the mouse. *Proceedings of the National Academy of Sciences of the United States of*  
752 *America*, 103(10), 3881–3886. <https://doi.org/10.1073/pnas.0505407103>
- 753 Chen, X., Li, X., Wong, Y. T., Zheng, X., Wang, H., Peng, Y., Feng, H., Feng, J., Baibado, J.  
754 T., Jesky, R., Wang, Z., Xie, H., Sun, W., Zhang, Z., Zhang, X., He, L., Zhang, N., Zhang,  
755 Z., Tang, P., ... He, J. (2019). Cholecystokinin release triggered by NMDA receptors  
756 produces LTP and sound-sound associative memory. *Proceedings of the National*  
757 *Academy of Sciences of the United States of America*, 116(13), 6397–6406.  
758 <https://doi.org/10.1073/pnas.1816833116>
- 759 Crestani, F., Keist, R., Fritschy, J. M., Benke, D., Vogt, K., Prut, L., Blüthmann, H., Möhler,  
760 H., & Rudolph, U. (2002). Trace fear conditioning involves hippocampal  $\alpha 5$  GABAA  
761 receptors. *Proceedings of the National Academy of Sciences of the United States of*  
762 *America*, 99(13), 8980–8985. <https://doi.org/10.1073/pnas.142288699>
- 763 Davis, M. (1992). The role of the amygdala in fear and anxiety. *Annual Review of Neuroscience*,  
764 15, 353–375. <https://doi.org/10.1146/annurev.neuro.15.1.353>
- 765 Egorov, A. V., Hamam, B. N., Fransén, E., Hasselmo, M. E., & Alonso, A. A. (2002). Graded  
766 persistent activity in entorhinal cortex neurons. *Nature*, 420, 173.  
767 <https://doi.org/10.1038/nature01171>
- 768 Esclassan, F., Coutureau, E., Di Scala, G., & Marchand, A. R. (2009). A Cholinergic-  
769 Dependent Role for the Entorhinal Cortex in Trace Fear Conditioning. *Journal of*  
770 *Neuroscience*, 29(25), 8087–8093. <https://doi.org/10.1523/JNEUROSCI.0543-09.2009>
- 771 Fransén, E. (2005). Functional role of entorhinal cortex in working memory processing. *Neural*  
772 *Networks*, 18(9), 1141–1149. <https://doi.org/10.1016/j.neunet.2005.08.004>
- 773 Fransén, E., Tahvildari, B., Egorov, A. V., Hasselmo, M. E., & Alonso, A. A. (2006).  
774 Mechanism of graded persistent cellular activity of entorhinal cortex layer V neurons.  
775 *Neuron*, 49(5), 735–746. <https://doi.org/10.1016/j.neuron.2006.01.036>
- 776 Fyhn, M., Molden, S., Witter, M. P., Moser, E. I., & Moser, M.-B. (2004). Spatial  
777 Representation in the Entorhinal Cortex. *Science*, 305(5688), 1258–1264.  
778 <https://doi.org/10.1126/science.1099901>
- 779 Gomez, J. L., Bonaventura, J., Lesniak, W., Mathews, W. B., Sysa-shah, P., Rodriguez, L. A.,  
780 Ellis, R. J., Richie, C. T., Harvey, B. K., Dannals, R. F., Pomper, M. G., Bonci, A., &  
781 Michaelides, M. (2017). Chemogenetics Revealed: DREADD Occupancy and Activation Via  
782 Converted Clozapine. *Science*, 357(August), 503–507.  
783 <https://doi.org/10.1126/science.aan2475>
- 784 Grider, M. H., Chen, Q., & David Shine, H. (2006). Semi-automated quantification of axonal

- 785 densities in labeled CNS tissue. *Journal of Neuroscience Methods*, 155(2), 172–179.  
786 <https://doi.org/10.1016/j.jneumeth.2005.12.021>
- 787 Hafting, T., Fyhn, M., Molden, S., Moser, M., & Moser, E. I. (2005). Microstructure of a spatial  
788 map in the entorhinal cortex. *Nature*, 436(7052), 801–806.  
789 <https://doi.org/10.1038/nature03721>
- 790 Han, C. J., O’Tuathaigh, C. M., van Trigt, L., Quinn, J. J., Fanselow, M. S., Mongeau, R., Koch,  
791 C., & Anderson, D. J. (2003). Trace but not delay fear conditioning requires attention and  
792 the anterior cingulate cortex. *Proceedings of the National Academy of Sciences of the*  
793 *United States of America*, 100(22), 13087–13092.  
794 <https://doi.org/10.1073/pnas.2132313100>
- 795 Hökfelt, T. (1991). Neuropeptides in perspective: The last ten years. *Neuron*, 7(6), 867–879.  
796 [https://doi.org/10.1016/0896-6273\(91\)90333-U](https://doi.org/10.1016/0896-6273(91)90333-U)
- 797 Jing, M., Zhang, Y., Wang, H., & Li, Y. (2019). G-protein-coupled receptor-based sensors for  
798 imaging neurochemicals with high sensitivity and specificity. *Journal of Neurochemistry*,  
799 151(3), 279–288. <https://doi.org/10.1111/jnc.14855>
- 800 Joseph, A., Tang, M., Mamiya, T., Chen, Q., Yang, L.-L., Jiao, J., Yu, N., & Tang, Y.-P. (2013).  
801 Temporal association of elevated cholecystokinergic tone and adolescent trauma is  
802 critical for posttraumatic stress disorder-like behavior in adult mice. *Proceedings of the*  
803 *National Academy of Sciences*, 110(16), 6589–6594.  
804 <https://doi.org/10.1073/pnas.1219601110>
- 805 Kim, W. Bin, & Cho, J.-H. (2017). Encoding of Discriminative Fear Memory by Input-Specific  
806 LTP in the Amygdala. *Neuron*, 95(5), 1129–1146.e5.  
807 <https://doi.org/https://doi.org/10.1016/j.neuron.2017.08.004>
- 808 LeDoux, J. E. (2000). Emotion Circuits in the Brain. *Annual Review of Neuroscience*, 23(1),  
809 155–184. <https://doi.org/10.1146/annurev.neuro.23.1.155>
- 810 Li, X., Yu, K., Zhang, Z., Sun, W., Yang, Z., Feng, J., Chen, X., Liu, C.-H., Wang, H., Guo,  
811 Y. P., & He, J. (2014). Cholecystokinin from the entorhinal cortex enables neural  
812 plasticity in the auditory cortex. *Cell Research*, 24(3), 1–24.  
813 <https://doi.org/10.1038/cr.2013.164>
- 814 Lilly, R., Cummings, J. L., Benson, D. F., & Frankel, M. (1983). The human Klüver-Bucy  
815 syndrome. *Neurology*, 33(9), 1141 LP – 1141. <https://doi.org/10.1212/WNL.33.9.1141>
- 816 Lopes, G., Bonacchi, N., Frazão, J., Neto, J. P., Atallah, B. V., Soares, S., Moreira, L., Matias,  
817 S., Itskov, P. M., Correia, P. A., Medina, R. E., Calcaterra, L., Dreosti, E., Paton, J. J., &  
818 Kampff, A. R. (2015). Bonsai: an event-based framework for processing and controlling  
819 data streams. *Frontiers in Neuroinformatics*, 9(April), 1–14.  
820 <https://doi.org/10.3389/fninf.2015.00007>
- 821 Maren, S. (2001). Neurobiology of Pavlovian fear conditioning. *Annual Review of*  
822 *Neuroscience*, 24(1), 897–931. <https://doi.org/10.1146/annurev.neuro.24.1.897>
- 823 Maren, S., & Fanselow, M. S. (1997). Electrolytic lesions of the fimbria/fornix, dorsal  
824 hippocampus, or entorhinal cortex produce anterograde deficits in contextual fear  
825 conditioning in rats. *Neurobiology of Learning and Memory*, 67(2), 142–149.  
826 <https://doi.org/10.1006/nlme.1996.3752>
- 827 McQuin, C., Goodman, A., Chernyshev, V., Kametsky, L., Cimini, B. A., Karhohs, K. W.,



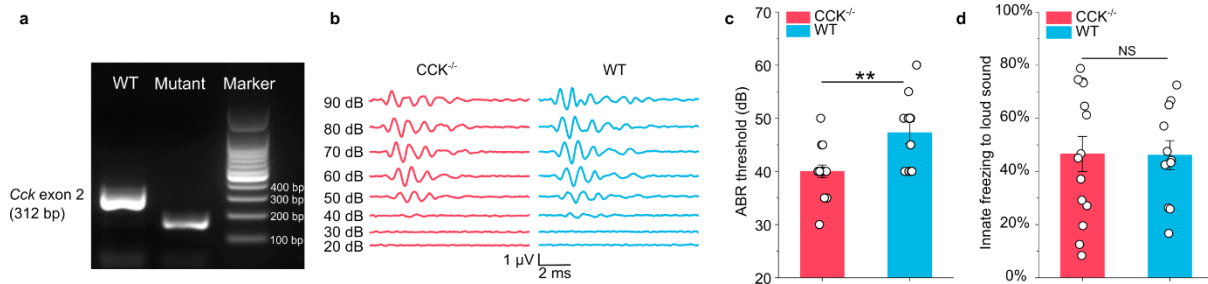
- 828 Doan, M., Ding, L., Rafelski, S. M., Thirstrup, D., Wiegraabe, W., Singh, S., Becker, T.,  
829 Caicedo, J. C., & Carpenter, A. E. (2018). CellProfiler 3.0: Next-generation image  
830 processing for biology. *PLoS Biology*, *16*(7), 1–17.  
831 <https://doi.org/10.1371/journal.pbio.2005970>
- 832 Nabavi, S., Fox, R., Proulx, C. D., Lin, J. Y., Tsien, R. Y., & Malinow, R. (2014). Engineering  
833 a memory with LTD and LTP. *Nature*, *511*(7509), 348–352.  
834 <https://doi.org/10.1038/nature13294>
- 835 Nauer, R. K., Whiteman, A. S., Dunne, M. F., Stern, C. E., & Schon, K. (2015). Hippocampal  
836 subfield and medial temporal cortical persistent activity during working memory reflects  
837 ongoing encoding. *Frontiers in Systems Neuroscience*, *9*(March), 1–13.  
838 <https://doi.org/10.3389/fnsys.2015.00030>
- 839 Pavlov, I. P. (1927). *Conditioned reflexes: an investigation of the physiological activity of the*  
840 *cerebral cortex*. Oxford Univ. Press.
- 841 Phelps, E. A., & LeDoux, J. E. (2005). Contributions of the amygdala to emotion processing:  
842 From animal models to human behavior. *Neuron*, *48*(2), 175–187.  
843 <https://doi.org/10.1016/j.neuron.2005.09.025>
- 844 Quirk, G. J., Reppas, J. C., & LeDoux, J. E. (1995). Fear conditioning enhances short-latency  
845 auditory responses of lateral amygdala neurons: Parallel recordings in the freely behaving  
846 rat. *Neuron*, *15*(5), 1029–1039. [https://doi.org/10.1016/0896-6273\(95\)90092-6](https://doi.org/10.1016/0896-6273(95)90092-6)
- 847 Rehfeld, J. F. (1978). Immunochemical studies on cholecystokinin. II. Distribution and  
848 molecular heterogeneity in the central nervous system and small intestine of man and hog.  
849 *Journal of Biological Chemistry*, *253*(11), 4022–4030.
- 850 Rogan, M. T., Stäubli, U. V., & LeDoux, J. E. (1997). Fear conditioning induces associative  
851 long-term potentiation in the amygdala. *Nature*, *390*(6660), 604–607.  
852 <https://doi.org/10.1038/37601>
- 853 Romanski, L. M., & LeDoux, J. E. (1992). Equipotentiality of thalamo-amygdala and thalamo-  
854 cortico-amygdala circuits in auditory fear conditioning. *The Journal of Neuroscience*,  
855 *12*(11), 4501–4509.
- 856 Runyan, J. D., Moore, A. N., & Dash, P. K. (2004). A Role for Prefrontal Cortex in Memory  
857 Storage for Trace Fear Conditioning. *Journal of Neuroscience*, *24*(6), 1288–1295.  
858 <https://doi.org/10.1523/jneurosci.4880-03.2004>
- 859 Ryou, J. W., Cho, S. Y., & Kim, H. T. (2001). Lesions of the entorhinal cortex impair  
860 acquisition of hippocampal-dependent trace conditioning. *Neurobiology of Learning and*  
861 *Memory*, *75*(2), 121–127. <https://doi.org/10.1006/nlme.2000.3966>
- 862 Saunders, A., Johnson, C. A., & Sabatini, B. L. (2012). Novel recombinant adeno-associated  
863 viruses for Cre activated and inactivated transgene expression in neurons. *Frontiers in*  
864 *Neural Circuits*, *6*(July), 1–10. <https://doi.org/10.3389/fncir.2012.00047>
- 865 Schindelin, J., Arganda-Carreras, I., Frise, E., Kaynig, V., Longair, M., Pietzsch, T., Preibisch,  
866 S., Rueden, C., Saalfeld, S., Schmid, B., Tinevez, J. Y., White, D. J., Hartenstein, V.,  
867 Eliceiri, K., Tomancak, P., & Cardona, A. (2012). Fiji: An open-source platform for  
868 biological-image analysis. *Nature Methods*, *9*(7), 676–682.  
869 <https://doi.org/10.1038/nmeth.2019>
- 870 Schon, K., Newmark, R. E., Ross, R. S., & Stern, C. E. (2016). A Working Memory Buffer in

- 871 Parahippocampal Regions: Evidence from a Load Effect during the Delay Period.  
872 *Cerebral Cortex*, 26(5), 1965–1974. <https://doi.org/10.1093/cercor/bhv013>
- 873 Shen, C.-J., Zheng, D., Li, K.-X., Yang, J.-M., Pan, H.-Q., Yu, X.-D., Fu, J.-Y., Zhu, Y., Sun,  
874 Q.-X., Tang, M.-Y., Zhang, Y., Sun, P., Xie, Y., Duan, S., Hu, H., & Li, X.-M. (2019).  
875 Cannabinoid CB1 receptors in the amygdalar cholecystokinin glutamatergic afferents to  
876 nucleus accumbens modulate depressive-like behavior. *Nature Medicine*, 25(2), 337–349.  
877 <https://doi.org/10.1038/s41591-018-0299-9>
- 878 Shin, L. M., Rauch, S. L., & Pitman, R. K. (2006). Amygdala, medial prefrontal cortex, and  
879 hippocampal function in PTSD. *Annals of the New York Academy of Sciences*, 1071, 67–  
880 79. <https://doi.org/10.1196/annals.1364.007>
- 881 Siegle, G. J., Thompson, W., Carter, C. S., Steinhauer, S. R., & Thase, M. E. (2007). Increased  
882 Amygdala and Decreased Dorsolateral Prefrontal BOLD Responses in Unipolar  
883 Depression: Related and Independent Features. *Biological Psychiatry*, 61(2), 198–209.  
884 <https://doi.org/10.1016/j.biopsych.2006.05.048>
- 885 Ventura, A., Meissner, A., Dillon, C. P., McManus, M., Sharp, P. A., Van Parijs, L., Jaenisch,  
886 R., & Jacks, T. (2004). Cre-lox-regulated conditional RNA interference from transgenes.  
887 *Proceedings of the National Academy of Sciences of the United States of America*, 101(28),  
888 10380–10385. <https://doi.org/10.1073/pnas.0403954101>
- 889 Xiong, W., MacColl Garfinkel, A. E., Li, Y., Benowitz, L. I., & Cepko, C. L. (2015). NRF2  
890 promotes neuronal survival in neurodegeneration and acute nerve damage. *The Journal of*  
891 *Clinical Investigation*, 125(4), 1433–1445. <https://doi.org/10.1172/JCI79735>
- 892 Zhang, G. W., Sun, W. J., Zingg, B., Shen, L., He, J., Xiong, Y., Tao, H. W., & Zhang, L. I.  
893 (2018). A Non-canonical Reticular-Limbic Central Auditory Pathway via Medial Septum  
894 Contributes to Fear Conditioning. *Neuron*, 97(2), 406-417.e4.  
895 <https://doi.org/10.1016/j.neuron.2017.12.010>
- 896 Zhang, Z., Xuejiao Zheng, C., Sun, W., Peng, Y., Guo, Y., Lu, D., Zheng, Y., Li, X.,  
897 Jendrichovsky, P., Tang, P., Ling He, S., Li, M., Liu, Q., Xu, F., Ng, G., Chen, X., & He,  
898 J. (2020). Visuoauditory associative memory established with cholecystokinin under  
899 anesthesia is retrieved in behavioral contexts. *The Journal of Neuroscience*, 1619–1673.  
900 <https://doi.org/10.1523/JNEUROSCI.1673-19.2019>

901

902

## 903 Supplementary Figures



904

### 905 Supplementary Figure S1. Genetic and behavioral examination of CCK<sup>-/-</sup> mice.

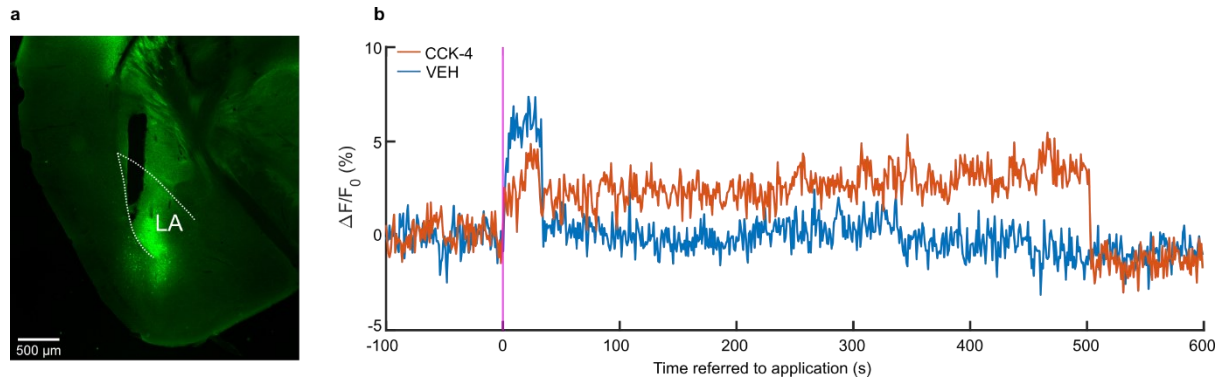
906 (a) PCR-based genotyping results showing the absence of the *Cck* exon 2 (312 bp) fragment in  
907 the mutant sample. The band in the mutant sample is a fragment of the CreER gene.

908 (b) Representative auditory brainstem response (ABR) traces from a CCK<sup>-/-</sup> mouse and a WT  
909 mouse, respectively.

910 (c) ABR thresholds in WT (N = 11) and CCK<sup>-/-</sup> (N = 15) mice. \*\*  $P < 0.01$ ; two-sample t-test.

911 (d) Innate freezing levels in WT (N = 14) and CCK<sup>-/-</sup> (N = 10) mice. NS, not significant;  $P >$   
912 0.05; two-sample t-test.

913



914

915 **Supplementary Figure S2. Exogenous CCK-4 activates CCKBR in the LA.**

916 **(a)** Verification of CCK-sensor2.0 expression and the optic fiber track in the LA.

917 **(b)** Representative traces of fluorescence signal of the CCK-sensor before and after the  
918 peripheral application (intraperitoneal injection) of CCK-4 (1 mM, 200 μL) or vehicle (VEH).  
919 Fluorescence signal was measured by fiber-photometry with an implanted optical fiber in the  
920 LA.

